Experimental and Numerical Studies of Nonsmooth Mechanical Systems

-Applications of Dimension Estimation

by

Johan Eriksson

April 2005 Licentiate Thesis from Royal Institute of Technology Department of Mechanics SE-100 44 Stockholm, Sweden

Akademisk avhandling som med tillstånd av Kungliga Tekniska högskolan i Stockholm framlägges till offentlig granskning för avläggande av teknologie licentiatexamen fredagen den 29:e april 2005 kl10.30i sal D3, Kungliga Tekniska högskolan, Valhallavägen 79, Stockholm. ©Johan Eriksson 2005

Abstract

When investigating the properties of real world mechanical systems, their dynamical behaviours are of importance. Most systems are found to have nonlinearities, due to e.g. the geometry of the system, nonlinear damping and stiffness in the materials, or the presence of friction and impacts between details in their design. Especially, nonsmooth systems with friction and impacts, which are examples of strong nonlinearities, can exhibit complex dynamics, and are the kind of systems considered in the present thesis. The focus of the thesis is on the complex response, better known as chaos, and in particular to characterise the response using the concept of fractal dimension. This allows an estimation of the minimum number of effective state variables of the underlying dynamical system, and can be used to distinguish between random and chaotic motion.

Two systems are considered; a simple impact oscillator setup and a pantograph from a railway train. Experimental measurements are compared with numerical simulations of mathematical models.

The oscillator consists of a pendulum excited by a shaker. Impacts between the two results in harmonic, subharmonic as well as chaotic responses for the pendulum's motion. A very good correlation between experimental and numerical results is found, and successful estimations of the attractors' dimensions are performed. The estimated dimensions are in agreement with the minimum number of state variables used in the mathematical model.

For the pantograph, various sources for nonlinearities are present, e.g. friction in the suspensions and the dampers, impacts in subsystems and at the excitation, and nonlinear characteristics of the air-suspension, which provides up-lift force to the pantograph's structure. A mathematical model is developed of a subsystem in the pantograph, and the results shows a qualitative good agreement with the experimental, with harmonic, subharmonic as well as chaotic responses. Frictional effects are found to be of significant importance, at low excitation frequencies, and the impacts are the major reason for chaotic response (for the cases investigated). Successful estimations of the attractors' dimensions are performed, indicating the need for a minimum of three to four state variables, depending on the attractor analysed, to describe the underlying dynamical system.

Keywords: Nonlinear dynamics, nonsmooth dynamics, discontinuities, friction, impact, chaos, correlation dimension, fractals

Contents

Preface							
1	Intr 1.1 1.2	Background	1 1 2				
2	Med 2.1 2.2 2.3	Chanical Systems Dynamical Systems	3 6 8 8				
3	Sys: 3.1	Impact Oscillator	11 12 12 13 13 15 16 17				
4	Sun 4.1	<i>y</i> 	21 22				
5	5 Discussion and Outlook						
Acknowledgement							

iv CONTENTS

Preface

This thesis considers the dynamics of systems with impacts and friction, and techniques for the analysis of data from experimental measurements and numerical simulations of such systems. An introduction to the field is given in the first chapters, using examples from the appended work as described below.

Report A. Johan Eriksson, 'Dimension Estimation of an Impact Oscillator, an Experimental and Theoretical Approach', (2004)

Paper A. Johan Eriksson, Arne B. Nordmark and Lars Drugge, 'An Experimental and Numerical Study of Pantograph Dynamics, with the Application of Dimension Estimation', (2005)

Chapter 1

Introduction

1.1 Background

In our daily life we all experience mechanical devices, such as trains, cars, motorbikes and bicycles. It is often that we do not reflect about the performance of the device, unless it breaks or there is a need for maintenance, and why should we be bothered? This is not the case for an engineer, who in the design stage of the product has to consider its future application, reliability, ease of repair and dynamic response. To enhance the understanding of a device, in the design stage or when modifying an existing design for better performance, engineers normally rely on the derivation and simulation of mathematical models. The complicity of the mathematical model depends on the aim of the investigation, e.g. if an existing product is to be evaluated and redesigned, a close correlation between the behaviour of the product and mathematical model is usually desired. If instead an investigation of certain phenomena's is carried out, a simplified model with the major characteristics of the system under consideration can fulfil the requirements. The reason to use a simplified model is that it contains less parameters, which opens up the possibility for a more detailed analysis of chosen parameters' importance. The latter choice of model is an approach commonly used in basic research.

Almost all real world products include nonlinearities, which for mechanical systems can be due to their geometrical design, the use of materials with nonlinear stiffness and damping, and friction and impacts between parts in the design. Mechanical systems with nonlinearities may exhibit complex behaviour and show sensitive dependence to changes in initial conditions, better known as chaos, and parameters. This argues for an investigation of the possible dynamics that can occur in the system under consideration. The development of realistic mathematical models rely on input from experimental data, since it is often not obvious which properties are of importance for the dynamics of the real system. When a good understanding of the system's characteristics is achieved, this information can be used in the derivation of new mathematical models or

when updating old ones. Simulations can then be performed to evaluate a new design, before building a real product, or in an investigation of the dynamics in an existing.

1.2 Scope and Aim

This work focuses on the nonlinear behaviour of mechanical systems with friction and impact. The systems are experimentally investigated and the results evaluated using numerical simulations of mathematical models. Nonlinear methods of data analysis, such as correlation dimension, are applied to the experimental and numerical time series data, to quantify the underlying dynamics of the mechanical systems under investigation. The aim of the studies is to analyse the effects nonlinear elements introduce into mechanical systems, and further the understanding of their importance in the development of mathematical models of the systems studied.

The research has been performed through the studies of two mechanical systems, as presented in Report A and Paper A in Appended Work. Report A consider an experimental and numerical study of an impact oscillator, previously investigated in Stensson and Nordmark [1], and the mathematical model is the same as derived and used in that study. A very good correlation was found between the experimental and numerical results. In Paper A a pantograph current collector from a railway train is considered. An experimental study of the pantograph is carried out and a mathematical model of a subsystem in the pantograph is derived and evaluated. The mathematical model successfully predicts the qualitative behaviours found in the experimental study, and the correlation dimension estimation is successful for applications to numerical as well as experimental data. Frictional effects are found to be of a major importance at low excitation frequencies and impacts are the reason for chaotic response of the system.

In the following chapters, a short introduction to the field of dynamical systems and the methods used when evaluating them is given, followed by a summary of the appended work. Finally a concluding discussion and recommendations for future work is given.

Chapter 2

Mechanical Systems

2.1 Dynamical Systems

Dynamical systems concerns the evaluation of systems in time, and there are two main types that are widely studied, Strogatz [2]; differential equations and iterated maps. The differential equations describe the system's continuous time evaluation and for iterated maps the time is discrete. Differential equations are the most commonly used method in science and engineering, with the major distinction between partial differential equations (PDE) and ordinary differential equations (ODE). The ODE's are only dependent on one variable, the time t, in difference with the PDE's, which depends on space as well as time variables. The ODE's are used in this work, and an example of the nonautonomous (time-dependent) equation of motion for a forced harmonic oscillator is given by a second-order ODE

$$m\ddot{x} + b\dot{x} + kx = F\cos\omega t,$$

where $\dot{x} = \frac{dx}{dt}$ and $\ddot{x} = \frac{d^2x}{dt^2}$. (2.1)

If three new variables are introduced, $x_1=x$, $x_2=\dot{x}$ and $x_3=\omega t$, the equation can be rewritten as

$$\dot{x}_1 = x_2
\dot{x}_2 = (-kx_1 - bx_2 + F\cos x_3)/m
\dot{x}_3 = \omega,$$
(2.2)

which is a three-dimensional autonomous system of first order equations. The equations are made autonomous by introducing the variable x_3 , i.e. time does not appear explicit in the equations any longer. The variables x_1 , x_2 and x_3 are referred to as state variables and their continuous time evaluation draws

a trajectory in a phase space, spanned by the coordinates x_1 , x_2 and x_3 . An example of a two dimensional projection of such a trajectory is seen in figure 1.

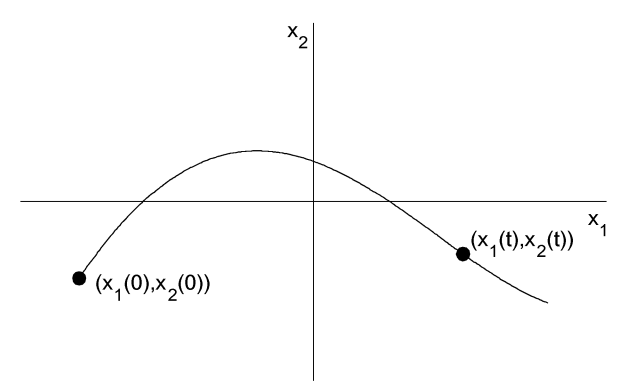


Figure 1. A phase space trajectory

The trajectory's long time evaluation in phase space forms the steady state solution of the dynamical system, the attractor. The dimension of this phase space is the same as the number of state variables needed to describe the dynamical system, in this case three. The dynamical system of can Eq. (2.2) be rewritten in a more general formulation as

$$\dot{\mathbf{x}} = \mathbf{f}(\mathbf{x}) \quad \mathbf{x} \in \mathbb{R}^n, \tag{2.3}$$

where \mathbf{x} is the state vector, \mathbf{f} is the forcing function and \mathbb{R}^n known as the state space, of dimension n. The complexity of the dynamical system depends on the dimension of the system and the smoothness and nonlinearity of the forcing function. The nonlinear system considered so far is referred to as smooth, with equations that are everywhere differentiable. Systems that experience sudden changes in state variables or the vector field, typically caused by impacts or friction, are known as nonsmooth. These kind of nonlinearities can be treated using events to switch vector fields or make jumps in state space, e.g. for the impact oscillator considered in Report A, where the impact is modelled using a coefficient of restitution and by switching the sign of the pendulum's velocity when impact with the excitation occur.

A very convenient property of a linear system is that it can be broken down into parts, which are solved separately using methods like Laplace transforms and Fourier analysis, before they are recombined into an answer (superposition). If instead a nonlinear system is considered, it is very hard or even impossible to obtain an analytical solution, thus they are normally analysed using numerical solutions or perturbation methods.

The response of a harmonically excited nonlinear system can, due to small changes in a parameter value, change its steady state period of motion. A one periodic response is a motion that repeats once every excitation cycle, in difference with a two periodic that repeats once every second excitation cycle, etc.

The latter case is an example of a subharmonic response, which is a motion that has a period n times the excitation's. If a system changes its response from one-to two-periodic motion, it has undergone a periodic doubling. Another possible response is quasiperiodic motion, of two fundamental frequencies. This corresponds to a motion of the trajectories on a closed two-dimensional torus in phase space. In the literature, quasiperiodicity and period doublings are reported as contributing factors that a system destabilises and its motion becomes chaotic, see for example Thomsen [3]. For impacting systems, low velocity "grazing" impacts, as analysed by Nordmark [4], can cause instability to the system, with possible chaotic motion as a result.

Impacting systems usually exhibit several attractors, with the result that different initial conditions can lead to completely different asymptotic behaviour. This argues for the importance to choose initial values that are representative for the real system under investigation. Chaotic systems are characterised by sensitive dependence on initial conditions, which is not the case for linear systems, whereby a small perturbation of the initial values will cause the trajectories to diverge exponentially fast as time evolves. An example of typical responses from an impact oscillator is seen in figure 2, review Report A for details.

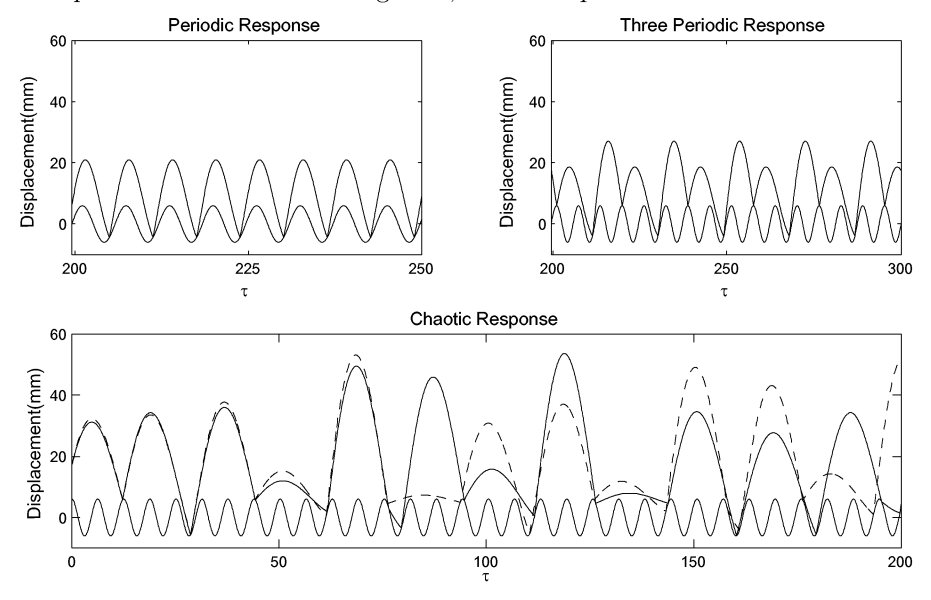


Figure 2. Numerical examples of time histories from an impact oscillator

The forcing of the oscillator is a harmonic sinusoidal signal and the impacts between the excitation and oscillator result in a periodic, subharmonic as well as chaotic response of the system. In the chaotic time history, an example of the divergence that occurs between two trajectories, due to a small perturbation in the initial values, is presented.

2.2 Graphical Representation of Results

In the analysis of nonlinear systems, it is convenient with graphical representation of the results. The time history is one way to do this, but when the motion becomes high-periodic or chaotic it is hard or even impossible to draw conclusions about the periodicity of the motion. An alternative is a two-dimensional projection of the state-space trajectories onto a phase plane, or the more powerful method by sampling a section of the phase plane trajectories once every excitation period. The latter representation is a Poincaré section, which reveals information of the periodicity of the motion and allows the investigator to distinguish between low dimensional chaos and truly random signals. The time histories earlier considered are presented by these techniques in figure 3, using a nondimensional relative displacement and velocity representation as defined in Report A.

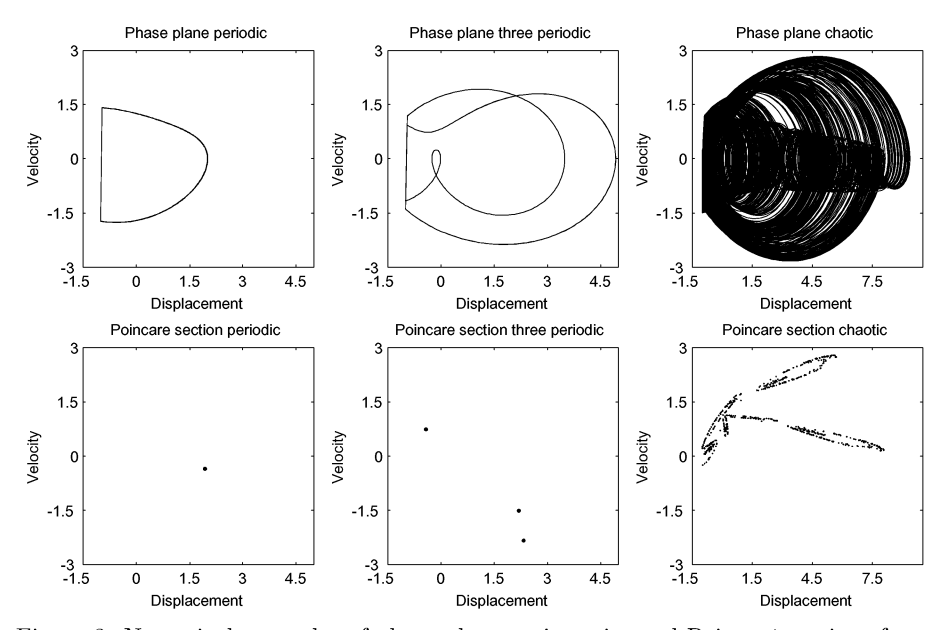


Figure 3. Numerical examples of phase plane trajectories and Poincaré sections from an impact oscillator

Analysing the figures, the trajectory of a one periodic motion draws a closed orbit in the phase plane, with a corresponding single point in the Poincaré section. For a change in parameter value, the motion becomes three periodic and the trajectory intersects with itself. The intersections of the trajectory are a result of projecting the dynamical system's attractor, based on three state variables, onto a surface. In the Poincaré section, where one dimension is removed due to the sampling of the trajectory, three points are seen and corresponds to the period of the motion. For the chaotic signal, the phase plane representation more or less fills the plane of projection, which indicates the need for an em-

bedding in three dimensions. If instead the attractor in the Poincaré section is analysed, a complex and irregular structure is observed, which has led people to call them strange. For an increasing amount of points, corresponding to a longer simulation time of the system, more and more details are added to its structure. If a small portion of the attractor is blown up, a sheet-like structure (fractal) that repeats for even smaller length scales is seen (self-similarity), but of course is limited by the resolution of the data. If a chaotic attractor, from a dynamical system of more than three state variables, is considered, the attractor would fill out a surface in the Poincaré section. Then, signs of the fractal structure or self-similarity will be hard to distinguish. This is an example of the limitation of the graphical representation, which is restricted to analysis of strange attractors that lives in a phase space of a maximum of three dimensions. Random and quasiperiodic motions are other responses that might appear as chaotic in the phase plane representation. If these responses are analysed in a Poincaré section, the random motion will fill a surface and the underlying dynamical system appear as high dimensional, in difference with the quasiperiodic response where the points that will form a closed curve.

In the analysis of a nonlinear dynamical system, an investigation of the response of the system for variations in parameter values is crucial. The bifurcation diagram is a representation used for this purpose, where a chosen variable's steady state response, sampled from a Poincaré section, is presented as a function of a chosen parameter. An example is given in figure 4, where the impact oscillator's Poincaré displacement data is presented as a function of excitation frequency.

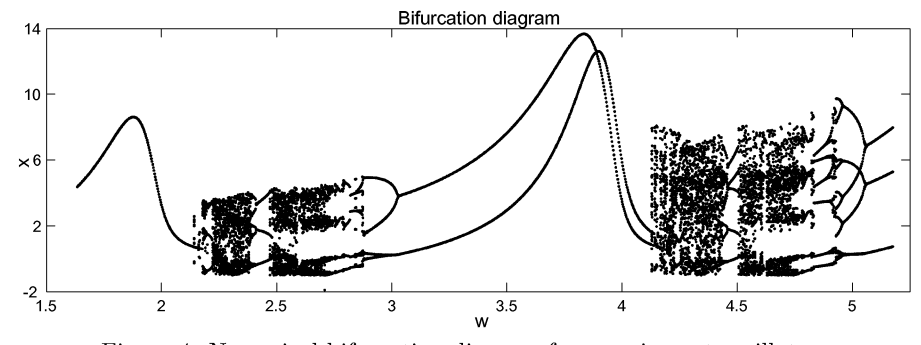


Figure 4. Numerical bifurcation diagram from an impact oscillator

Analysing the figure, information about periodicity of the motion, regions of chaotic motion and the presence of periodic windows is obtained. Although the graphical methods discussed can give indications for the presence of chaotic motion, there is a need for more sophisticated methods to rule out that the analysed motion does not come from an attractor of high periodic, random or quasiperiodic motion.

2.3 Analysis of Results using Fractal Dimension

Traditional linear methods, like power spectrum analysis, will give a broad spectrum of frequencies for chaotic motion and the results are hard to quantify. If instead nonlinear methods, like Lyapunov exponents and fractal dimension, are applied more information can be revealed from the motion analysed. The Lyapunov exponent is a measure of the exponential divergence for nearby chaotic trajectories due to their sensitive dependence on initial conditions, as discussed above, i.e. chaotic motion has a positive Lyapunov exponent. For a more detailed review of the concept and how to apply it to an experimental time series see Kantz and Schreiber [5].

Fractal dimension provides a way to quantify the self-similarity in a geometrical object, and the dimension is a measure of the minimum number of state variables needed to describe the underlying dynamical system. If the time series data from the attractors in figure 3 are analysed, the one- and three-periodic responses will yield a dimension d=1, and the chaotic motion a noninteger dimension between d=2 and 3. The noninteger dimension is evidence for a fractal attractor, and the dimension known as fractal dimension. If the value is rounded to the next higher integer, the minimum number of state variables is obtained. In the dimension estimation of an attractor from a quasiperiodic signal, of two fundamental frequencies, a dimension d=2 is expected. The reason for this is that the trajectories are attracted to a surface in phase space.

If instead a random signal is considered, the dimension will be equivalent to the phase space the signal is embedded in. The reason for this is that the points will fill its full embedding space, and this property of fractal dimension can be used to distinguish between random and chaotic motion.

Several estimators exist that can be used in the measurement of the fractal attractor's dimension, e.g. capacity dimension, similarity dimension, Haussdorf dimension, information dimension, pointwise dimension and correlation dimension. Farmer et al. [6], gives a detailed review and investigates different estimators, and in many cases they yield a similar result. A trajectory on a fractal attractor can visit some of the attractor's regions more often than others. This is not accounted for in the capacity, similarity and Haussdorf dimension that only considers the geometry of the attractor. The information and correlation dimension accounts not only for the geometry of the attractor, but also the frequency the trajectory visits its different sections. The correlation dimension is used in the investigations performed in this work, and a short review of the method is given below.

2.3.1 Pointwise and Correlation Dimension

In the estimation of the correlation dimension, the Grassberger and Procaccia [7] approach is the most commonly used due to its efficiency compared to other methods. The general procedure of the estimator is as follows; a ball of radius ε is centred at x on the attractor, as exemplified in figure 5.

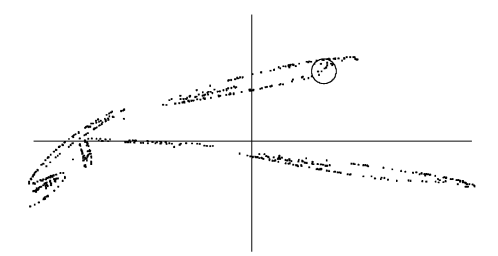


Figure 5. Numerical Poincaré section from an impact oscillator

Now let $N_x(\varepsilon)$ denote the number of points on the attractor inside the ball, then the number of points in the ball typically grows as a power law when increasing the value of ε

$$N_x(\varepsilon) \propto \varepsilon^{d_x},$$
 (2.4)

where d_x denotes the pointwise dimension at x. Since the value for the pointwise dimension can vary significantly over the attractor one averages $N_x(\varepsilon)$ over many points x and the resulting $C(\varepsilon)$ is known as the correlation sum

$$C(\varepsilon) = \frac{2}{N(N-1)} \sum_{i=1}^{N} \sum_{j=i+1}^{N} \Theta(\varepsilon - \|\mathbf{x}_i - \mathbf{x}_j\|), \qquad (2.5)$$

where Θ is the Heaviside step function, $\Theta(x)=0$ if $x \leq 0$ and $\Theta(x)=1$ for x>0. The sum counts the pairs $(\mathbf{x}_i - \mathbf{x}_j)$ whose distance is smaller than ε . For an infinite amount of data $(N \longrightarrow \infty)$ and for small ε , the resulting $C(\varepsilon)$ is expected to scale as a power law

$$C(\varepsilon) \propto \varepsilon^d,$$
 (2.6)

and the correlation dimension d can be defined as

$$d(N,\varepsilon) = \frac{\partial \log C(\varepsilon, N)}{\partial \log \varepsilon}$$
 (2.7)

$$d = \lim_{\varepsilon \to 0} \lim_{N \to \infty} d(N, \varepsilon). \tag{2.8}$$

The calculation of the correlation sum involves, by definition, the use of phase space vectors as locations of the points on the attractor. Since it is seldom the case that all the relevant variables can be measured in an experimental set-up, there is a need for attractor reconstruction. Takens [8] showed that it is possible to reconstruct the full dynamics in an auxiliary phase space, using the method of delay vectors. A sampled time series of a chosen variable, y_n , is used for this purpose

$$\mathbf{x}_n = (y_{n-(m-1)\tau_d}, y_{n-(m-2)\tau_d, \dots, y_{n-\tau_d}}, y_n), \tag{2.9}$$

where \mathbf{x}_n is the observable state variable at discrete time n, τ_d is the delay time and m is referred to as the embedding dimension. The method has been shown to yield reliable information for the understanding of the underlying dynamical system, if the dynamical invariant set is low-dimensional and the noise level is low. The delay time is in this work chosen primarily as the first zero-crossing of the auto-correlation function in combination with visual inspection of the reconstructed attractor embedded in two-dimensions.

Once the attractor is reconstructed by the embedding procedure, the estimation of the correlation dimension is performed in two steps. First the correlation sum $C(\varepsilon)$, Eq. (2.5), is determined for a range of ε , where the minimum value is below the noise level of the original signal, y_n , and the maximum value typically the magnitude of the signal, for several values of m. The next step is to inspect $C(m,\varepsilon)$ for indications of self-similarity, which corresponds to the power law region in a plot of $\log C(\varepsilon)$ vs. $\log \varepsilon$. The self-similarity is even better visualised by the plateau in the plot of $d(N,\varepsilon)$ vs. $\log \varepsilon$. If the indications are convincing a value for the correlation dimension can be estimated. The box-assisted approach suggested by Kantz and Schreiber [5] is used in this work. The algorithm was chosen due to its simplicity, and if the points in the data set are not too clustered the operation count will be $\propto N$ for N points. It is generally faster than multidimensional trees, if the data sets are low-dimensional, which can achieve a performance with the number of operations proportional to $N \log N$. If the correlation sum is evaluated directly, as two nestled loops, it will contain about $N^2/2$ terms for N points. This naive implementation was initially considered, but the computation was found to be very time consuming.

Chapter 3

Systems Studied

The first of the two experimental systems considered is a simple impact oscillator set-up, designed for the investigation of certain phenomena's that occur in impacting systems, Stensson and Nordmark [1]. The oscillator consists of a pendulum and a shaker, which provides forcing to the system through a moving impact surface. The second system is a pantograph current collector, Schunk WBL88/X, which provides electric power to a railway train from the overhead catenary system. The pantograph is an engineering system, built up by a frame linkage that supports a head frame, at which carbon collector strips are attached. An example of the device, on the roof of an X2000 train, is seen in figure 6.



Figure 6. A pantograph current collector on the roof of an X2000 train

3.1 Impact Oscillator

The schematic design of the impact oscillator is seen in figure 7. The oscillator consists of a pendulum, built up by a metal sphere (4) and a leaf spring (3), with an initial clearance to a base (2). The base is attached to a shaker (1), which provides sinusoidal forcing to the system, and is massive in comparison with the metal sphere. The reason to make it massive is to minimise the effects of impact on its motion.

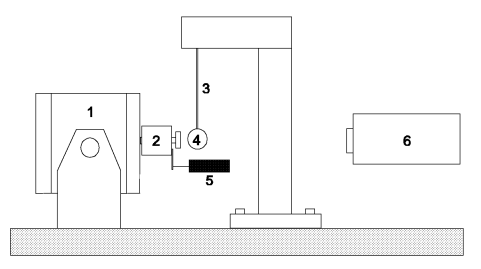


Figure 7. The schematic design of a simple impact oscillator's experimental setup

3.1.1 Experiment

In the experimental set-up of the impact oscillator, a displacement transducer, (5) in figure 7, measures the motion of the base. An additional measurement of its velocity is provided through a laser (6). The velocity of the pendulum mass is measured with a second laser, also placed at (6), and the displacement data achieved through integration.

When performing experimental measurements, it is crucial to have a good understanding of the characteristics of the system considered. With some prior knowledge, it is easier to evaluate the different behaviours found and to conclude about their origin. It is also of importance to get realistic parameters from the system if numerical models are to be developed. With this in mind, preparatory experimental measurements were carried out in order to characterise the system. From free decay measurements of the pendulum, the natural frequency and damping could be determined. The coefficient of restitution was estimated from measurements of the relative velocity between pendulum and base, before and after impact. In the measurements of the system's response, the following procedure was used. The amplitude of the shaker was initially increased until impact with the pendulum occurred. The transients were allowed to die out before a measurement was recorded, followed by a step change in the frequency and the procedure's latter part repeated. The responses found in the system were harmonic, subharmonic as well as chaotic.

3.1.2 Modelling

The mathematical model of the impact oscillator is the model previously derived in Stensson and Nordmark [1], with the significant parameters presented in figure 8.

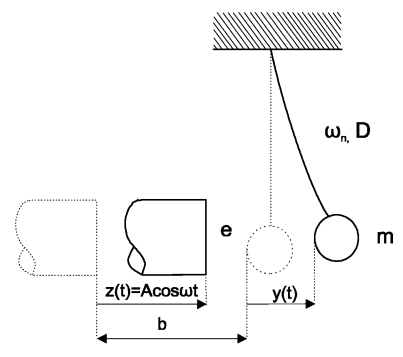


Figure 8. The significant parameters for the mathematical model

In the model, the base provides harmonic excitation to the pendulum's mass, m. Small deflections are assumed of the leaf spring, at which the mass is attached, whereby a linear model can be used. The distance marked with b in the figure corresponds to the equilibrium standoff distance between the mass and the base, i.e. the excitation is provided through impacts between the two. In the model, the impacts are modelled using a coefficient of restitution, e, which assumes an instantaneous change in velocity when impacts occur

$$v_{out} = -ev_{in}, (3.1)$$

where v_{in} is the relative velocity before impact and v_{out} the corresponding velocity after impact. The coefficient e then represents the loss of energy in the impact, and the impact law introduces a nonsmooth nonlinearity into the model. The dynamics of the system are assumed to be dominated by the first mode of the beam, since the other modes will be damped out quickly, whereby an ordinary differential equation can be formulated to describe the dynamics of the system. The equation is given in a non-dimensional form, based on the natural frequency and the equilibrium standoff distance, see Report A. For details about the derivation of the equation and an extensive review of the system's dynamics, from experimental and numerical investigations, see Stensson and Nordmark [1].

3.1.3 Examples of Results

The results presented in figure (2)-(5) are all from numerical simulations of the impact oscillator. In figure 9, w=3.98, the corresponding experimental result for the chaotic attractor is presented, but in a different scaling of the figure. The numerical attractor, w=2.56, in figure 9 is to be compared with the experimental, w=2.34, in the same figure.

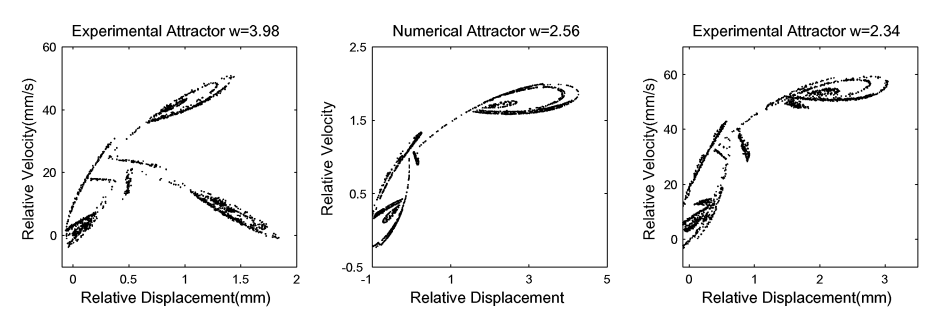


Figure 9. Experimental and numerical Poincaré sections from an impact oscillator

The experimental and numerical results does not show a perfect match for the parameter values used, but the agreement between the structure of the attractors must be considered as very good.

An example from a dimension estimation, performed on the experimental w=2.34 attractor is presented in figure 10.

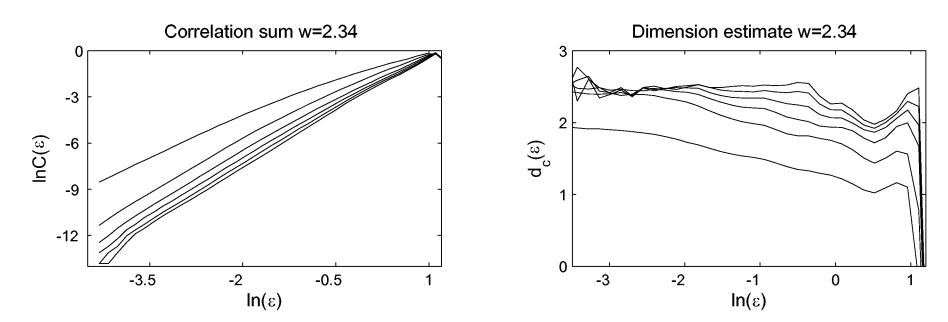


Figure 10. Correlation sum log/log plot and dimension estimation from the experimental attractor at w=2.34

Time series data was used in the estimation and analysing the plateau, found in the scaling region -3<ln(ε)<-2, in the dimension estimate plot a fractal dimension $d_c \approx 2.5 \pm 0.05$ can be estimated.

3.2 Pantograph

The pantograph's schematic design is seen in figure 11. It consists of a head and frame assembly, where the frame assembly consists of two frames, an upper (8) and a lower (9) that connects to one another, the ground and the head frame (1) with y-axis rotational joints. An air-spring provides up-lift force to the structure, and two friction dampers (11) are attached between the lower frame (9) and the ground. A third friction damper (7) connects between the upper (8) and head frame (1). The design, where a bar link (10) connects from the lower frame (9) to the ground, restricts the head frame's motion to displacement along the z-axis.

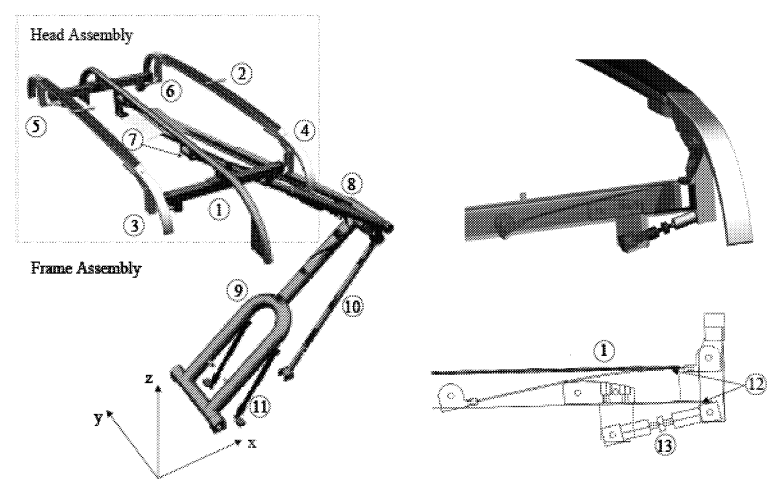
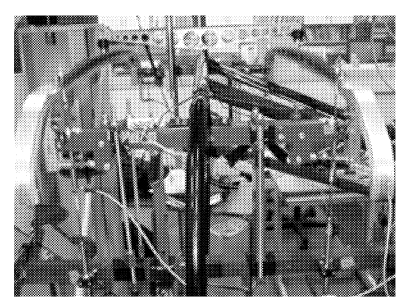


Figure 11. Schematic view of the pantograph assembly, where (1) is the head frame, (2) a carbon collector strip, (3)-(6) suspensions, (7) the connection point for the friction damper between upper and head frame, (8) upper frame, (9) lower frame, (10) bar link, (11) friction dampers and the location of the air-suspension, (12) the leaf springs and (13) is one of the rigid links.

The head assembly includes two carbon collector strips, where the one marked (2) is referred to as the contact strip back (cs_b) and the other as the contact strip front (cs_f) , and a head frame (1), at which the strip ends are suspended. The suspensions are built up by leaf springs (12) and rigid links (13), which allow an x-rotational and z-translational motion of the strip, and their location on the strip referred to as the left (3)(4) and right (5)(6) side $(cs_{fl}, cs_{bl}, cs_{fr}, cs_{br})$. The motion of the strip is limited by the head frame in upward displacement, referred to as the upper limit, and a lower leaf spring (12) in downward displacement, referred to as the lower limit, introducing a piecewise linear stiffness in the suspension.

3.2.1 Experiment

In the experimental set-up, a hydraulic actuator, marked (1) in figure 12, was placed in a rigid foundation built around the pantograph. The actuator provides sinusoidal excitation of the pantograph, applied at the contact strips, through an aluminium beam (3). The motion of the excitation is measured by an internal displacement transducer in the hydraulic actuator, and contact sensors (2) indicate when the lower limits are reached or if contact loss occurs between the excitation beam and the strips.



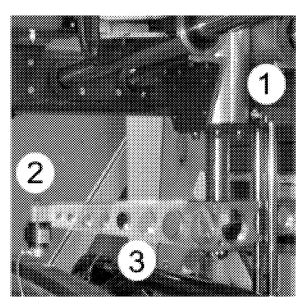




Figure 12. The experimental set-up, where (1) indicates the hydraulic actuator, (2) is one of the excitation contact sensors, (3) is the aluminium excitation beam and (4) one of the inductive displacement transducers.

At each of the contact strips suspensions and head frame's ends, inductive displacement transducers are located (4). The ones attached to the contact strip measures its displacement vs. the head frame and the ones attached to the head frame measures displacement vs. ground.

In the preparations, before evaluating the systems response, measurements were performed to provide information about the system's characteristics. The suspensions were investigated to find the corresponding stiffness in the different regions for the; free leaf spring, lower limit and upper limit, that produces a piecewise linear stiffness of the suspension. The friction in the suspensions was estimated from free decay measurements of the contact strip, and found to vary significantly depending on the amount of force used when attaching them to the head frame and contact strip. To measure the contact strip's inertia, it was pivoted at its centre of mass and springs with known stiffness attached at each of its ends. Free decay measurements were performed, from which the contact strip's inertia could be estimated.

In the experimental runs, the excitation of the pantograph was applied at the centre of the contact strips. To better understand the complex dynamics of the pantograph, the head frame was fixed to ground in some of the measurement cases. In the measurements, the pantograph was excited at a fixed amplitude and frequency for some time, to allow transients in the dynamics to die out, before a recording was performed. A step change in frequency was undertaken and the same procedure repeated. A dynamical system can have more than one response at a certain frequency, something that might be missed using the

present method of frequency sweep, and could possibly had been found starting with the same initial conditions or perturbing the pantograph during run.

In the measurement results, harmonic, subharmonic as well as chaotic and possible quasiperiodic responses were found.

3.2.2 Modelling

The mathematical model represents the experimental case when the head assembly is fixed to ground, without considering the frame assembly, and limited to one contact strip. The reason to restrict the model to the head assembly is that is it desirable to find out whether a simple model can be used to predict the complex dynamics, found in the experimental measurements on the pantograph. The model consists of a rigid beam, which represents the contact strip, with rotational and translational freedom around its centre of mass. The beam is suspended at it ends in suspensions with piecewise linear stiffness, friction and viscous damping. The friction is modelled using a smooth step-function for a more efficient numeric handling. The viscous damping model is a result of fitting numerical results to experimental, and its force decay for increased velocity.

An additional mass m_2 is included in the model to represent a bending oscillation in the beam, as a result of experimental measurements indicating that such a frequency is excited in the contact strip during run. In figure 13 a schematic picture of the subsystem is presented, and seen from the front, i.e. what appears to be the right side is actually left.

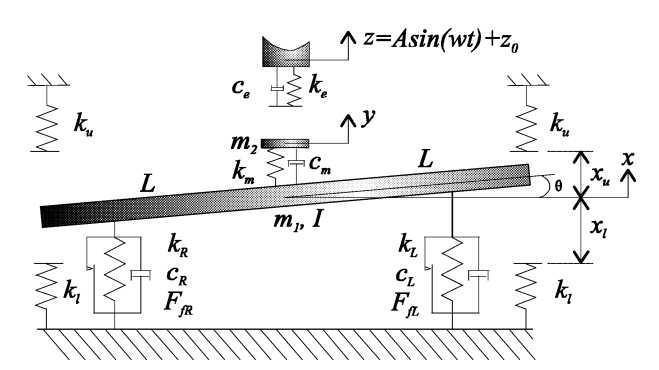


Figure 13. Schematic drawing of the mathematical model, with significant parameters

The excitation of the model is provided through a stiff mass-less spring and damper element, providing a force at the mass m_2 , which allows loss and impact between the contact strip and excitation.

In difference with the impact model for the impact oscillator, the impact is here modelled using a smoother model. The excitation's spring provides a force as long as the mass m_2 is in contact with the excitation, in difference with its viscous damper that only provides force under compression. The upper

and lower limits are modelled as linear stiff springs, and provide force when the beam's end is in contact. The mathematical model, represented by three second-order differential equations is found in Article A.

3.2.3 Examples of Results

Some examples of results from the pantograph investigation are now to be given. The results come from the experimental case when the head frame is fixed to ground, and are comparable with the numerical results. In the first example, as seen in figure 14, the upper row corresponds to experimental results and the lower to numerical simulations.

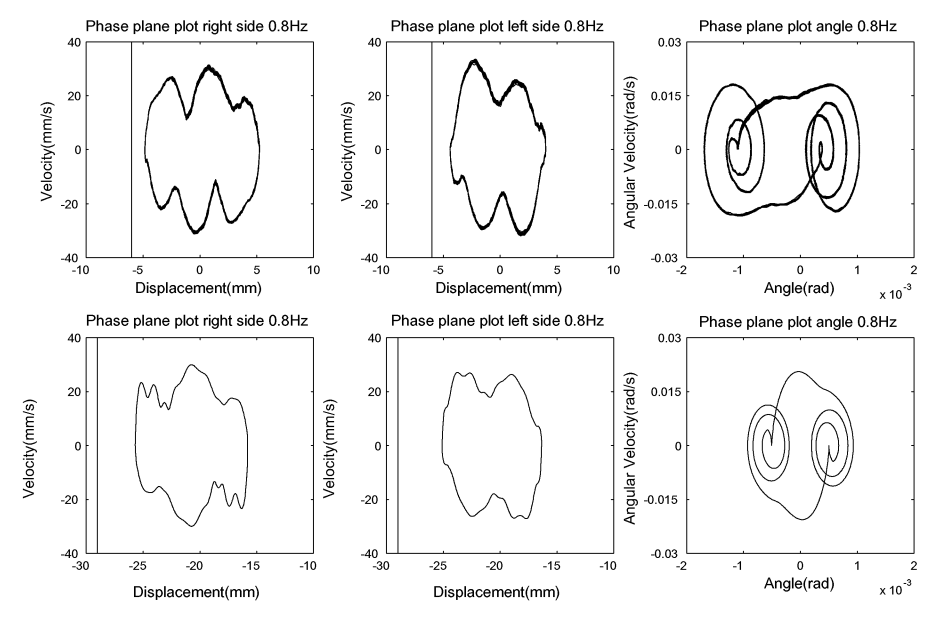


Figure 14. Experimental and numerical results from the pantograph, ω =0.8Hz

The response is seen to be periodic, and with a similar behaviour in the experimental as in the numerical results. The oscillations in the velocity data is an effect of the friction force, which is seen to have a significant effect on the contact strip's motion at this frequency.

In the next example the motion is chaotic, as seen in figure 15.

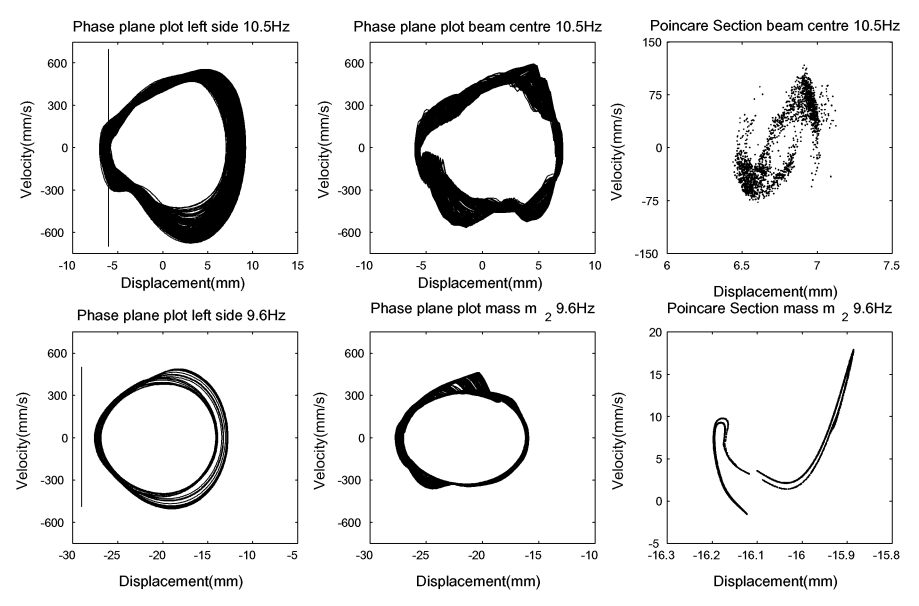


Figure 15. Experimental and numerical results from the pantograph, ω =10.5Hz and ω =9.6Hz

The figure with the measurement from the beam centre is seen to have similar dynamics to the corresponding simulation, with results from the mass m_2 .

An example of a dimension estimation, when applied to numerical Poincaré data, is seen in figure 16. The true scaling region is found in the region $-4 < \ln(\varepsilon) < -2.5$, and an estimation of the fractal dimension in this region yields $d_c = 1.2 \pm 0.1$. This corresponds to a dimension $d_c = (1+1.2) \pm 0.1$ for the underlying dynamical system.

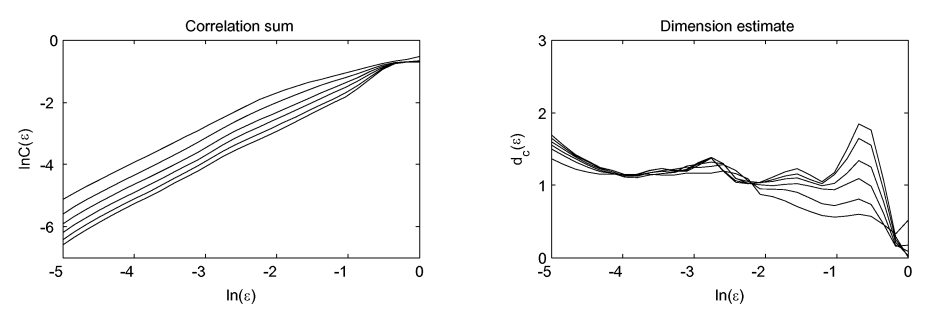


Figure 16. Log/log plot of the correlation sum and the dimension estimate using numerical Poincaré data

Chapter 4

Summary of Appended Work

As a preliminary investigation, to test the experimental procedures and the algorithms for data analysis, a system known to exhibit chaos was chosen, as presented in **Report A**. The system is a simple impact oscillator set-up, which consist of a pendulum with an initial clearance to its excitation, provided by a shaker. The system is known to exhibit grazing and chaotic motion, and are behaviours found in the results from the experimental investigation. Two major regions with chaotic behaviour are found within the frequency range analysed, and periodic windows occurs within these. A very good agreement in the structure of the experimental and numerically obtained attractors is found, but there was a marked parameter value offset between the two. The focus of this report is on the application of dimension estimation to the chaotic signals, experimental as well as numerical, in order to estimate the fractal dimension of the attractors. The correlation dimension is chosen for this purpose, due to its efficiency among other estimators, and applied to a single time series, reconstructed in an embedding space using the method of delay coordinates. The results are compared with estimations from Poincaré sections, which showed similar results. The estimations using experimental and numerical data convincingly support that the underlying dynamical system lives in a three dimensional state space. These results, in combination with the convincing correlation, in the structure, between numerical and experimental attractors supports the assumption that the system's dynamics is dominated by the first mode of the pendulum's beam. This was an assumption made by Stensson and Nordmark [1], in the design of the mathematical model, based on an ordinary differential equation.

In **Paper A**, a pantograph from a railway train is investigated, which in difference with the system in Report A is an engineering system. The pantograph was experimentally investigated, and a mathematical model of a subsystem was developed and numerically analysed. The nonlinearities in this system are mainly impacts and friction in suspension elements, friction in dampers, loss

and impacts at the excitation and nonlinear characteristics in an air-spring. The friction in the suspension elements was found to have a significant effect on the behaviour of the contacts strip for low excitation frequencies. At higher frequencies the impacts at the excitation and upper limits are the reasons for subharmonic and chaotic response of the system. This was found to be the case for the full system as well as for the subsystem. The importance of including rotational as well as translational degrees of freedom for the contact strip in the mathematical model is demonstrated by the experimental and numerical studies of the system. When exciting the system near a translational natural frequency of the strip/spring configuration, large amplitudes occur for the contact strips' and the lower frame's motion. Excitation near a rotational natural frequency results in a marked decrease in the amplitude response of one side of the contact strip's motion together with increased amplitude for the other side. The experimental investigation of the full system and for the subsystem showed harmonic, subharmonic as well as chaotic and possible quasiperiodic behaviour. In the numerical simulations harmonic, subharmonic and chaotic response was found, but the possibility for quasiperiodic motion is not ruled out since investigations of similar mathematical models, Jerrelind and Stensson [9], has reported the presence of this behaviour.

4.1 Authors Contribution

Report A

J. Eriksson (JE) carried out the work with helpful guidance and feedback from A. B. Nordmark (AN).

Paper A

All authors contributed in the planning of the experimental work, characterisation of the system and analysis of the data.

JE performed the dimension estimations, experimental measurements, numerical simulations, and developed the mathematical model on the basis of the results from the characterisation of the system.

The manuscript was prepared by JE, with feedback from AN and L. Drugge.

Chapter 5

Discussion and Outlook

This thesis considers the analysis of two nonsmooth mechanical systems, which are expected to exhibit complex behaviours due to the presence of strong non-linearities from friction and impacts. Chaotic responses have previously been reported in systems with these characteristics, and the focus of this work is particularly on the characterisation of this behaviour using fractal dimension estimation. In the dimension estimations, correlation dimension was chosen and implemented as the box-assisted approach proposed in Kantz and Schreiber [5]. The algorithm was successfully applied to time series and Poincaré data, from experimental measurements and numerical simulations of mathematical models, and predicted the minimum number of state variables to be used to describe the underlying dynamical system.

The systems studied are a simple impact oscillator set-up and a pantograph current collector from a railway train. From the results it is confirmed that it is of importance to consider the possibility of complex response in systems where impact between different parts is likely to occur. In the analysis of these systems, simulations of mathematical models have been shown to predict the behaviours found in the experimental systems.

The impact oscillator set-up is, due to its simplicity, suitable for experimental analysis of impact phenomena. It is known to exhibit regions of chaotic motion, and periodic windows within these. In impacting systems, grazing bifurcations can result in destructive large amplitude motion. The same impact oscillator set-up is being used in ongoing research for the application of control to this phenomena.

Experimental investigations of the pantograph considered the full system, as well as a subsystem. Nonlinearities from friction and impacts substantially affected the contact strips' responses, and activated rotational as well as translational motions in them. Resonance in the strip/spring configuration also affected the strips' behaviour, and resulted in large amplitude motion of the head frame for low excitation frequencies. The lower frame's motion was typically out of phase with that of the excitation and contact strips above the first resonance in the system, and this resulted in impacts at the excitation for lower frequencies

than in the study of the subsystem. Impacts are the major reason for chaotic motion of the contact strip, for the cases considered. An oscillation of the contact strip's centre point was found to be present from the measurements, most likely to have its origin in bending of the strip. The oscillation was taken account for in a mathematical model of the subsystem, by including an additional mass at the centre of the strip. The model is developed on the basis of experimental measurements and includes the essential nonlinearities, found to be from impacts and friction, and has rotational as well as translational degrees of freedom. The model can be enhanced to represent the full pantograph system, but before this can be done there is a need for further experimental characterisation of the system. The lower frame's characteristics should be considered in this analysis, and the impact and damping models updated with parameters from a more detailed investigation. Another aspect to consider is the origin of the oscillation found in the contact strip that was assumed to be due to bending, since the possibility that a natural frequency is excited in the system responsible for providing excitation is not ruled out. When a mathematical model of the full pantograph system has been developed, more realistic forcing situations should be considered and the model evaluated with experimental measurements.

Although successful dimension estimations of the fractal attractors, numerical and experimental, have been performed, the application of the estimator did not turn out to be straight forward. The estimations from experimental attractors were applied to inductive transducer and laser data, with low noise level and statistics from up to 6500 excitation cycles. Different samplings of the signals, using Poincaré data as well as time series data with more than 40 points/excitation cycle, and variations in the embedding parameters were taken into account. Still problems arise in the estimations, with the lack of convincing plateaus indicating self-similarity in the attractor. The same problems arise for the application to numerical data, from simulations using tight error tolerances, with statistics from up to 12000 excitation cycles.

In some of the estimations, the application to Poincaré data resulted in the most reliable results, and for others no convincing plateaus could be found. The same was the case for applications to time series data. No rule of thumb in the dimension estimation procedure can be concluded, since the parameters and samplings to be used depend on the attractor under consideration. Another drawback of the estimator is that the amount of data that can practically be evaluated is limited due to the computing time. The problems, in combination with the need for repeated estimations before convincing results are obtained, are limitations of the estimator. The limitations and the practical implementation of the results are aspects that have to be addressed before the concept of fractal dimension can be more widely used for engineering purposes.

For the studied systems, the most convincing plateaus were found for the application to the attractors from the impact oscillator, and the results argued for the need to represent the dynamics in a three dimensional phase space. The same results were found for the application to experimental data from the pantograph, but the attractors from numerical simulations indicated the need for a phase space of three to four dimensions, depending on the attractor analysed.

Acknowledgement

First of all I would like to thank my supervisor Docent Arne Nordmark. It has been a pleasure to work with you and take part of your enthusiasm and knowledge within the field of mechanics.

I would like to express my gratitude to my co-author Dr. Lars Drugge. Thanks for generously sharing your experience within the field of applied mechanics.

Kent Lindgren and Danilo Prelevic at the Marcus Wallenberg Laboratory for Sound and Research, I am grateful for all the help during the experimental investigations. It has been a real pleasure to work with you in the laboratory.

The financial support from the Swedish Research Council (VR) is gratefully acknowledged.

Professor Annika Stensson, thanks for providing feedback during the investigations performed on the pantograph.

I would like to express my gratitude to my former and present colleagues at KTH, and especially the people on the 8th floor at the Department of Mechanics. All the jokes and pointless discussions resulted in a warm and friendly atmosphere at the office, thanks!

Daniel Ahlman and Jenny Jerrelind, thanks for reading and providing feedback on the manuscript of this thesis.

My godson Lukas, Pia, Milan and Andreas, I am so thankful for having you in my life!

Finally, thanks to my friends and family. I have been neglecting you during the past months and I hope that we can spend more time together from now on.

Stockholm, March, 2005

Johan Eriksson

Bibliography

- [1] A. Stensson and A. B. Nordmark, 'Experimental investigation of some consequences of low velocity impact in the chaotic dynamics of a mechanical system'. Philosophical Transactions of Royal Society of London A, vol.347, pp.439-448, (1994).
- [2] S. H. Strogatz, 'Nonlinear Dynamics and Chaos', Westview Press, ISBN 0-7382-0453-6 (2000).
- [3] J. J. Thomsen, 'Vibrations and Stability', 2:nd edition, Springer Verlag Berlin Heidelberg New York, ISBN 3-540-40140-7, (2003).
- [4] A. B. Nordmark, 'Effects Due To Low Velocity Impact In Mechanical Oscillators', International Journal of Bifurcations and Chaos, vol.2, pp.597-605, (1992).
- [5] H. Kantz and T. Schreiber, 'Nonlinear Time Series Analysis', Cambridge Nonlinear Science Series 7. ISBN 0-521-65387-8, (1999).
- [6] F. D. Farmer, E. Ott and J. A. Yorke, 'The Dimension of Chaotic Attractors', Physica D, vol.7, pp.153-180, (1983).
- [7] P. Grassberger and I. Procaccia, 'Measuring the Strangeness of Strange Attractors', Physica D, vol.9, pp.189-208, (1983).
- [8] F. Takens, 'Detecting Strange Attractors in Turbulence', Lecture Notes in Math. 888, Springer-Verlag, pp.366-381, (1981).
- [9] J. Jerrelind and A. Stensson, 'Nonlinear dynamic behaviour of coupled suspension systems', Meccanica, 38, pp 43-59, (2003).

Report A

Dimension Estimation of an Impact Oscillator, an Experimental and Theoretical Approach

Technical report, Department of Mechanics, Royal Institute of Technology,

KTH, SE-100 44 Stockholm, Sweden

Johan Eriksson 2004

Abstract

An experimental and numerical study of the dynamics in an impact oscillator has been carried out. Two major regions of chaotic motion were found within the frequency range analysed and periodic windows occurred within these. The numerically obtained attractors were in good agreement with the experimental, with a very similar structure, but for a marked difference in frequency. The chaotic signals were analysed using the method of correlation dimension, in order to estimate the fractal dimensions of the attractors. In the dimension estimation, based on the use of a single time series and the method of phase space reconstruction, the theoretical results verified the experimental and argued for a fractal dimension $d\approx 2.4\pm 0.1$. The estimations were compared with the ones coming from a single Poincaré section, and similar results were achieved. Rounding the estimated value to the next higher integer gives a prediction that the dynamics live in a three dimensional phase space, in agreement with the number of states used for modelling the mathematical model.

1 Introduction

In this report a numerical and experimental study of the dynamics in a simple impact oscillator set-up has been carried out. The dynamics of the attractors was reconstructed in an auxiliary phase space, using a single time series, and their fractal dimensions estimated using the method of correlation dimension [1].

The dynamical system's continuous time evolution can be described by a set of first-order autonomous ordinary differential equations

$$\frac{dx}{d\tau} = u$$

$$\frac{du}{d\tau} = -\frac{2D}{w}u - \frac{1}{w^2}x + a\left\{\left(1 - \frac{1}{w^2}\right)\cos\theta + \frac{2D}{w}\sin\theta\right\}$$

$$\frac{d\theta}{d\tau} = 1$$
(1)

If initial conditions are given to the states (x, u, θ) , the trajectory of the system can be determined. The system discussed shows phase space contraction, due to the damping term, and the long time solutions of such a system can be described by attracting sets in phase space, the attractors.

If no forcing is applied to the system the attractor will typically be an orbit in phase space. If instead periodic forcing is applied, the attractor can exhibit a very complex and much more irregular structure, which has led people to call them strange. The attractor is then better known as a fractal and their existence in a physical context was first shown by [2].

The dimension of a dynamical system corresponds to the number of states needed to fully uncover the system's dynamics, in this example the three described above. If the dimension of an attractor is evaluated, the orbit would yield a dimension one to be compared with the fractal that has a non-integer number between two and three. If the non-integer value is rounded to the next higher integer, the number of states needed to describe the dynamics is achieved.

The method of correlation dimension has become the most popular when estimating the fractal dimension of an attractor, due to its relatively high computational efficiency and that it is easy to implement. The method has successfully been applied within various fields, such as gearbox fault diagnosis [3] and rolling bearing condition monitoring [4]. The reason for using it is that a prediction of how many state variables that is needed to describe the underlying dynamical system can be estimated, which in combination with the ability of the estimator to distinguish between random or chaotic motion provides useful information for engineers when modelling dynamical systems.

2 Experiment

2.1 The Experimental Setup

The experimental rig contains a mass, coming from a steel ball bearing, attached to a spring made out of shim steel with dimensions $0.5x12.9x160 \text{ mm}^3$. Two shim steel beams with thickness 0.1mm were attached to the spring, using double-sided adhesive tape, in order to increase the damping.

The external forcing of the mass is achieved using an electro-magnetic shaker from Brüel & Kjaer, type 4809, and was sinusoidal. A large mass, referred to as the base, was attached to the shaker armature. This in order to make the base massive in comparison with the pendulum's, marked (4) in figure 1, and minimise the effects of impacts on the motion of the excitation. The impact head is made out of aluminium in order to avoid magnetic effects from the shaker. The different parts of the experimental setup can be seen in figure 1.

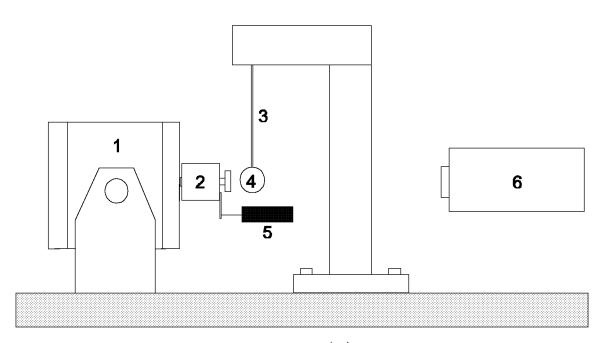


Figure 1. The experimental setup. Number (1) is the electro-magnetic shaker, (2) is the base, (3) is the spring, (4) is the mass, (5) is the inductive displacement transducer and (6) are the lasers.

The motion of the base was measured in [V/mm] using an inductive displacement transducer, Solartron DFG5.0, and the velocity measured in [V/(mm/s)] using a laser, Polytec PDV100. The velocity of the ball was measured in [V/(mm/s)] with a laser, Polytec OFV303, and the displacement automatically integrated in the same equipment. The signal generation and the collection of the data were performed using a dynamic signal and system analyzer from Siglab, sampling the signals from the measurement devices with 2.56kHz, connected to a computer with a measurement card, SlimSCSI 1460D, from Adaptec. The power amplifier connected to the electro-magnetic shaker, is from Brüel & Kjaer, type 2718.

When measuring data in an experimental system there will always be sources of errors, such as noise and resolution of the AD-converter.

2.2 The Experimental Methodology

At a fixed frequency the amplitude of the shaker was increased until the base impacted with the mass, initially at rest. The system was run for some time to

allow a warm up before the measurements were started. Then the frequency was increased in steps and an investigation of the motions occurring at the different frequencies carried out. Some time were given between the measurements, after a step change in frequency, to allow for the transient effects to die out and possible parameter drift to stabilise.

Two different standoff distances were investigated, I: b=0.2mm and II: b=0.5mm, which must be considered as approximate values since they were hard to measure exactly and might vary during the experimental run, especially after a resonance peak. The frequencies investigated spanned from $w \approx 1.9$ -4.4.

No filtering has been applied to the measured time series used in the dimension estimations, but the results presented in the next section has been filtered using a 3 point averaging filter to smoothen up the trajectories.

2.3 Examples of Experimental Results

Four different ways of presenting the results will be used here: time histories, phase-plots, Poincaré sections and bifurcation diagrams. The bifurcation diagram is simply a way to give an overview of the systems behaviour under the variation of a parameter, here represented by the displacement component of the Poincaré data versus the frequency ratio w. The Poincaré data is collected whenever the phase of the excitation is $\pi/2 \pmod{2\pi}$, in the equations of motion (corresponding to the time when the base passes the equilibrium position, going from positive to negative displacement). The relative displacement and velocity between the mass and the base is used in the phase- and Poincaré plots to allow for comparison with results from the mathematical model. The impact occurs for x=0 in the experimental data, but due to the difficulties in the integration of the velocity data a minor variation is noticed. The bifurcation diagrams for standoff distance I and II are shown in figure 2.

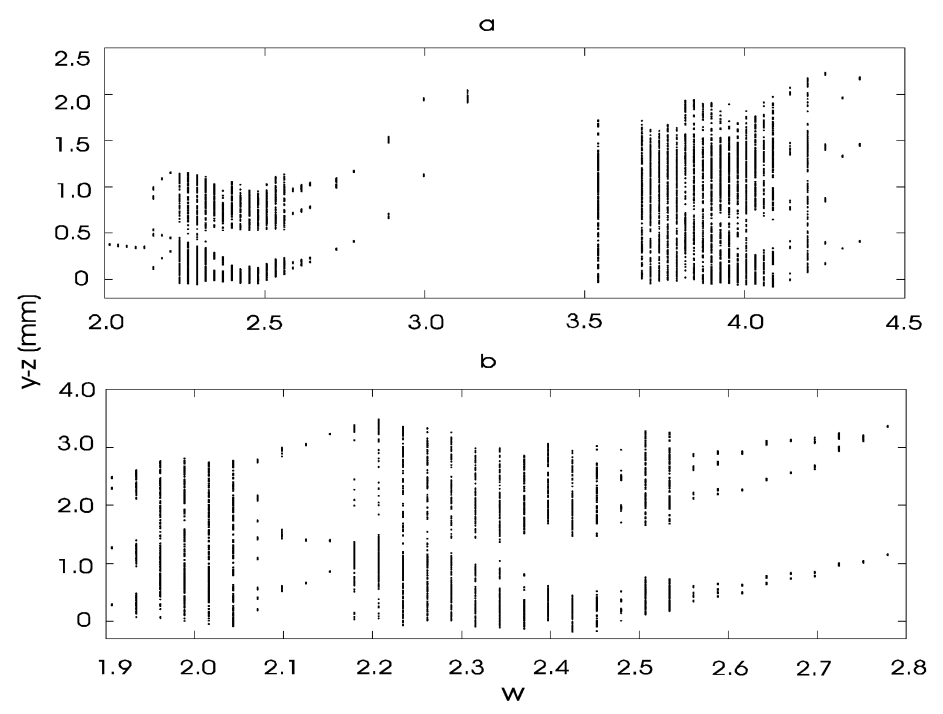


Figure 2. Experimental bifurcation diagrams. (a) Standoff $I: b{=}0.2$ mm, (b) Standoff $II: b{=}0.5$ mm

In the bifurcation diagrams, two major regions for chaotic motion occurred, and periodic windows within these. A single dot at a certain frequency corresponds to a period one motion, two dots to a period two motion etc. The variables y and z on the axis in the plot represents the motion of the mass respectively the motion of the ball.

Looking closer into the motion at a frequency in the first chaotic regime for standoff distance II, here w=2.34. Figure 3(a) shows a typical time history of the system, where the periodically oscillating curve corresponds to the base motion and the other curve represents the resulting chaotic motion of the mass.

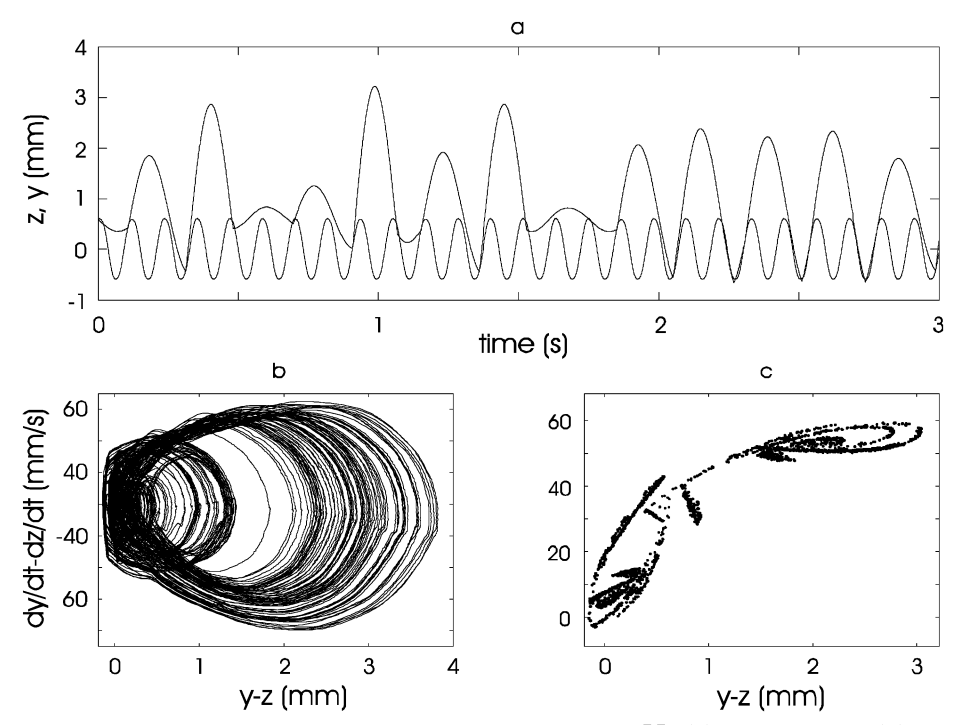


Figure 3. Chaotic signal at w=2.34, standoff distance II. (a) Time history, (b) Phase plot, (c) Poincaré section

In the phase plot, figure 3(b), a discontinuous change in velocity can be detected at the moment of impact between the ball and base. The attractor in figure 3(c) shows a curled up fingerlike structure, which is a sign of the mass undergoing a rapid series of impacts and a common behaviour in impacting systems.

If a frequency w=3.98, in the second chaotic regime for standoff distance I, is analysed, a second finger appears on the attractor in figure 4(a), due to the increased sampling in the Poincaré section.

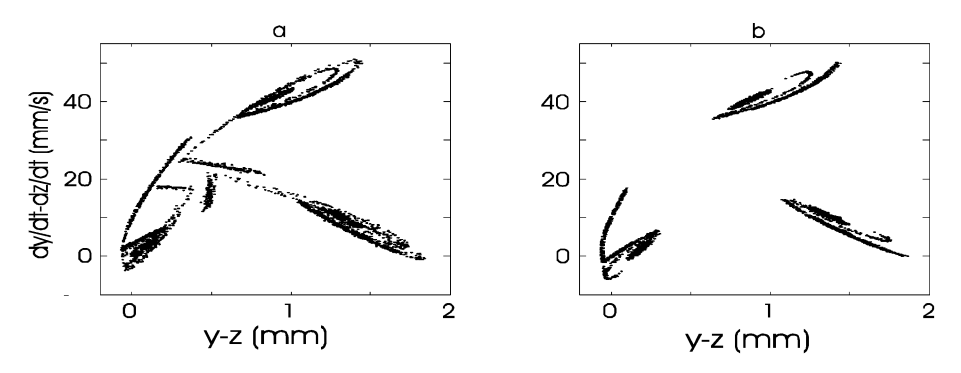


Figure 4. Experimental attractors standoff distance I, (a) w=3.98, (b) w=4.03

For w=4.03 and standoff distance I, figure 4(b), the attractor has divided up into three disconnected structures. The sharp corners indicate that the mass undergoes low velocity impacts, so called "grazing". Looking into a typical time series for this frequency, the low velocity- and rapid series of impacts can be identified in the region 0.05 < t < 0.1 in figure 5(a).

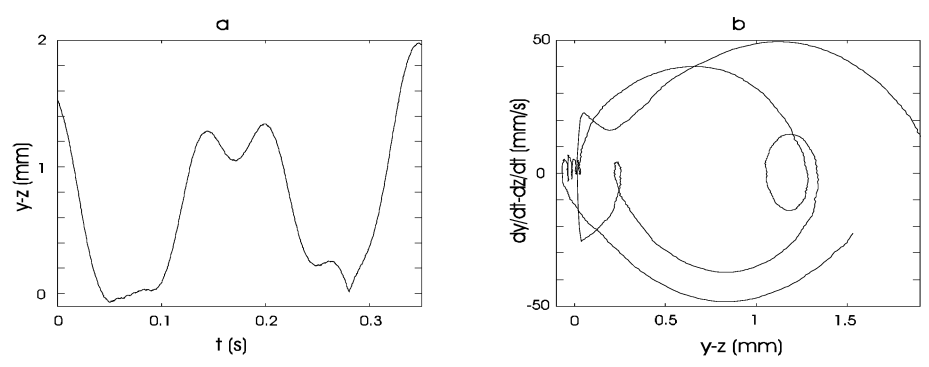


Figure 5. Experimental signal at w=4.03, standoff distance I. (a) Time history, (b) Phase plot

The noise and problems in the integration procedure makes it hard to distinguish the impacts in the time history, but if the region around zero velocity and displacement in the phase plot, figure 5(b), is analysed a clearer picture of the discussed behaviour is seen.

3 Numerical Simulation of the System

3.1 The Mathematical Model

The mathematical model of the mechanical system considered in this report is based on the use of an impact law. The impact law introduces a discontinuous change in velocity at the moment of impact between the mass and base, which is moving harmonically at a fixed frequency. The mass is attached to a spring/beam, which is assumed to be linear for small deflections and the equilibrium distance between the mass and the base is called b.

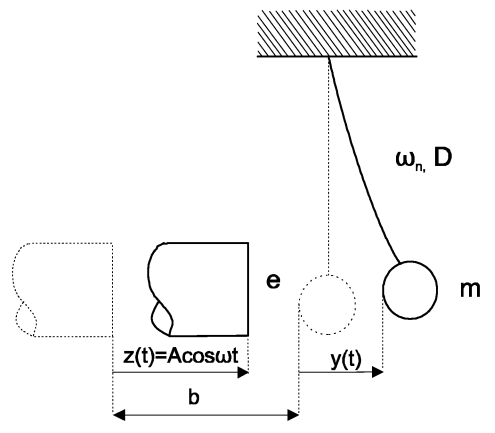


Figure 6. The significant parameters

The higher modes of the beam are quickly damped out, whereby an assumption is made that the dynamics of the system is dominated by the first mode. Therefore an ordinary differential equation can be derived for the system [5], and is given in a non-dimensional form based on the natural frequency and the equilibrium standoff distance:

$$\frac{d^2x}{d\tau^2} + \frac{2D}{w}\frac{dx}{d\tau} + \frac{1}{w^2}x = a\left\{\left(1 - \frac{1}{w^2}\right)\cos\tau + \frac{2D}{w}\sin\tau\right\}$$

$$x \geq -1$$

$$\left(\frac{dx}{d\tau}\right)_{\text{just after impact (at x=-1)}} = -e\left(\frac{dx}{d\tau}\right)_{\text{just before impact (at x=-1)}} \tag{2}$$

where

x(t) = (y-z)/b, the non-dimensional displacement

 $z(t) = A\cos(\omega t)$, the motion of the base [m]

y(t) = the motion of the mass [m]

b = the equilibrium distance between mass and base [m]

e = the coefficient of restitution

 ω_n = the undamped natural frequency of the mass/beam system [rad/s]

a = A/b, the non-dimensional amplitude ratio

 $w = \omega/\omega_n$, the non-dimensional frequency ratio

D = the non-dimensional damping ratio

 $\tau = \omega t$, the non-dimensional time

3.2 Simulations

The bifurcation diagram in figure 7 was made by numerically solving the differential equations with an ode45 solver in the Matlab software package, using the non-dimensional frequency ratio as a bifurcation parameter. The Poincaré displacement data was collected using an event function, after the transients had died out. The values of the non-dimensional parameters were calculated according to the experimental measurements, see Appendix

e=0.82 D=0.078 and a=1.1

The initial conditions used were x(0)=1, $dx/d\tau(0)=1$.

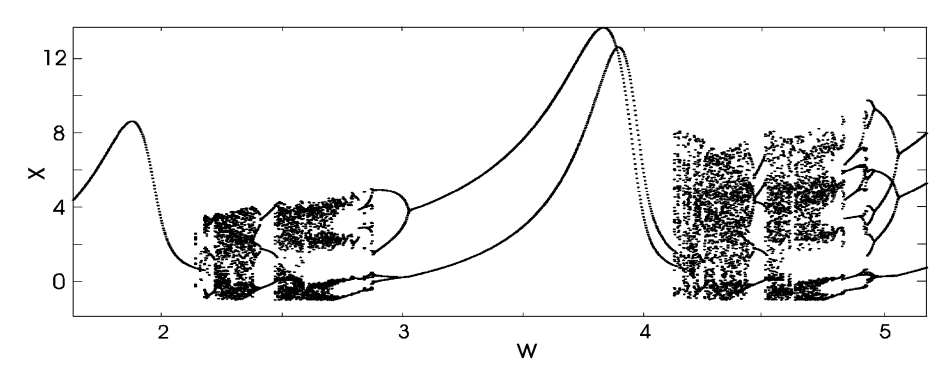


Figure 7. Numerical bifurcation diagram

The same characteristics as for the experimental diagrams are seen, with two major regions of chaotic motion and periodic windows within these. The attractors from the Poincaré sections were analysed at the different frequencies in the bifurcation diagram, in order to look for similarities with the ones coming from the experiment. A perfect match was not achieved between the experimental and numerical results, where the chaotic regimes are pushed towards slightly higher frequencies than in the experiment. This can be due to uncertainties in the measured parameter values, which might change with the forcing frequency. Although a good match with the experimental attractors is found for the frequencies w=2.56, 4.52 and 4.68 as seen in figure 8.

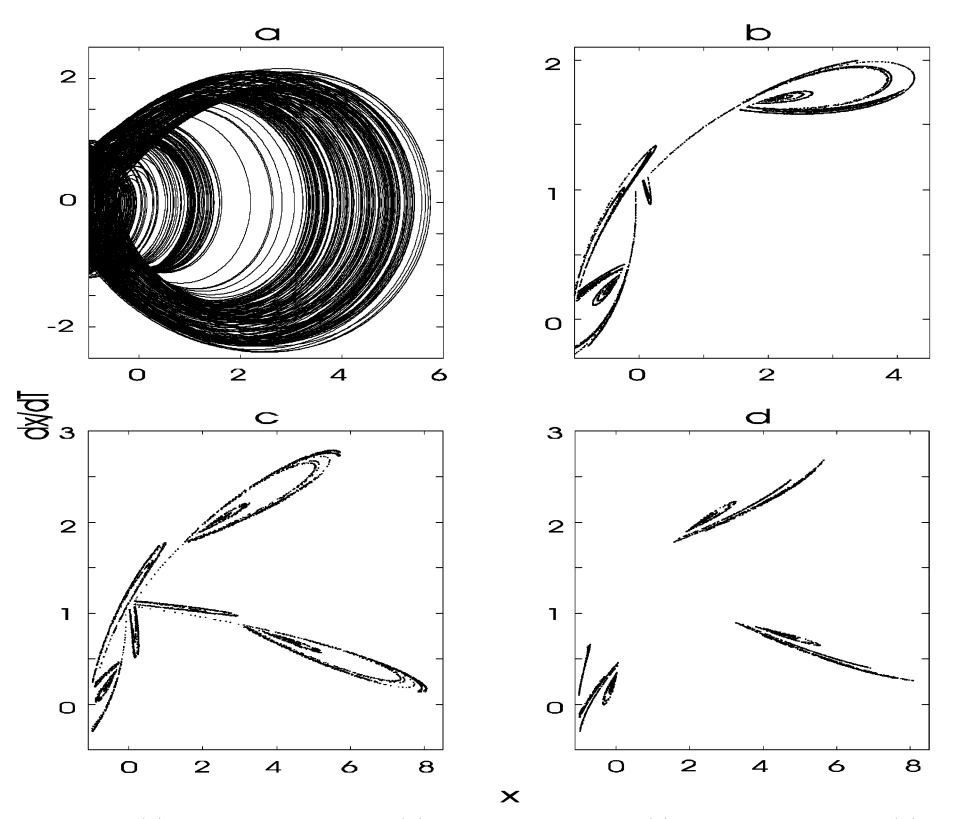


Figure 8. (a) Phase plot w=2.56, (b) Attractor w=2.56, (c) Attractor w=4.52, (d) Attractor w=4.68

4 Dimension

4.1 Fractal Dimension

Fractal dimension is a way to quantify the self-similarity of a geometrical object. There are many different ways to do this for a fractal set, and more information about the methods can be found in for example [6] and [8]. One way is using the method of correlation dimension, introduced by [1], which has become a standard due to its efficiency compared to others.

4.2 Pointwise and Correlation Dimension

The Grassberger-Procaccia approach is to fix a point x on the attractor. If $N_x(\varepsilon)$ denotes the number of points on the attractor inside a ball of radius ε about x, then the number of points in the ball typically grows as a power law when increasing the value of ε

$$N_x(\varepsilon) \propto \varepsilon^{d_x},$$
 (3)

where d_x denotes the pointwise dimension at x. Since the value for the pointwise dimension can vary significantly over the attractor one averages $N_x(\varepsilon)$ over many points x and the resulting $C(\varepsilon)$ is known as the correlation sum. The basic formula is

$$C(\varepsilon) = \frac{2}{N(N-1)} \sum_{i=1}^{N} \sum_{j=i+1}^{N} \Theta(\varepsilon - \|\mathbf{x}_i - \mathbf{x}_j\|), \tag{4}$$

where Θ is the Heaviside step function, $\Theta(x)=0$ if $x \leq 0$ and $\Theta(x)=1$ for x>0. The sum counts the pairs $(\mathbf{x}_i - \mathbf{x}_j)$ whose distance is smaller than ε . For an infinite amount of data $(N \longrightarrow \infty)$ and for small ε , C is expected to scale as a power law

$$C(\varepsilon) \propto \varepsilon^d,$$
 (5)

and the correlation dimension d can be defined as

$$d(N,\varepsilon) = \frac{\partial \ln C(\varepsilon, N)}{\partial \ln \varepsilon} \tag{6}$$

$$d = \lim_{\varepsilon \to 0} \lim_{N \to \infty} d(N, \varepsilon). \tag{7}$$

4.3 Correlation Sum from a Time Series

The calculation of the correlation sum involves, by definition, the use of phase space vectors as the locations of points on the attractor. In an experimental rig it is seldom the case that all the relevant variables can be measured. The most common way to solve this problem is to reconstruct the full dynamics in an auxiliary phase space, using a continuously sampled time series of a single variable and the method of delay coordinates, as introduced by [7]

$$\mathbf{x}_n = (x_{n-(m-1)\tau_d}, x_{n-(m-2)\tau_d, \dots, x_{n-\tau_d}}, x_n), \tag{8}$$

where \mathbf{x}_n is the observable state variable at discrete time n, τ_d is the delay time and m is referred to as the embedding dimension. The method has been shown to yield reliable information for the understanding of the underlying dynamical system, if the dynamical invariant set is low-dimensional and the noise-level is low.

4.3.1 Embedding

The most important embedding parameter in attractor reconstruction is $m\tau_d$, i.e. the product of the embedding dimension and the delay time. Choosing a

good window $m\tau_d$ highly affects the calculation of d and for some choices a measurable plateau, indicating self-similarity in the data for $d(N, \varepsilon)$, is completely absent even when examining high-quality data, see [9].

In [7] it was shown that the reconstructed attractor almost always is topologically equivalent to the original state space of a dynamical system, as long as m>2d+1. Although other studies have shown that many systems can be embedded in fewer dimensions.

In practice a value is chosen for the delay time τ_d and then the dimension d is calculated for increasing m. In theory the choice of τ_d , considering infinite and noise-free data, is arbitrary [10] [6]. Since infinite and noise-free data do not occur in reality a good choice facilitates the analyses. There is no trivial choice for τ_d , but for too small values problems with strong correlations between successive elements of the delay vectors occur, and all the vectors x_n are clustered around the diagonal in the \mathbb{R}^m , unless m is very large. For too large values of τ_d the vectors will be unrelated and the points will fill the \mathbb{R}^m , destroying the fractal structure of the attractor confined to small length scales.

Many authors suggest the use of mutual information [11] or the auto-correlation function when determining the optimal τ_d , but [9] shows that none of them are consistently successful.

In this report, the first zero crossing of the auto-correlation function has primarily been used, in combination with visual inspection of the attractor in a two-dimensional embedding. The τ_d obtained with this method has been compared with the value for the first minimum of the mutual information function, and should give a good estimate for finding a compromise between the extremes of too small and too large τ_d . Even though a good estimate of τ_d might have been found it must be verified that d is consistent under reasonable changes in the embedding procedure.

Once the attractor is reconstructed by the embedding procedure the estimation of the correlation dimension is performed in two steps. First the correlation sum $C(\varepsilon)$, Eq. (4), is determined for the range of ε , where the maximum value is chosen according to the magnitude of the signal and the minimum somewhere below the noise-level in the data, for several values of m. The next step is to inspect $C(m,\varepsilon)$ for indications of self-similarity. If the indications are convincing a value for the correlation dimension can be estimated.

4.3.2 Temporal Correlations

The estimator, Eq. (4), has been shown to be biased towards too small dimensions, due to temporal correlations of the data when the pairs entering the formula are not statistically independent. This is due to the fact that data which is close in time is also close in space, as an effect of the continuous time evolution. In the estimation of correlation dimension the geometrical structure of the fractal attractor and the frequency at which the dynamically independent trajectories visits various sectors in phase space are to be analysed. If care is not taken pairs from dynamically dependent trajectories will enter the algorithm. These have nothing to do with the attractor's fractal structure and will result

in a serious underestimation of the dimension. The behaviour is exemplified in figure 9, where a 2-D projection of a reconstructed attractor is shown. The circles represents different values for ε and A and B are different points for which the algorithm is trying to find neighbours.

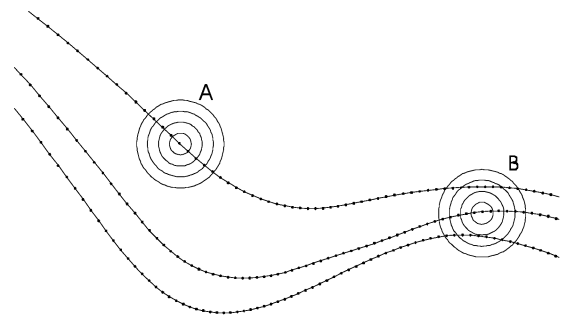


Figure 9. Temporal correlations

For point B there are still some neighbouring points on dynamically independent trajectories, while all the neighbouring points for A are on the same trajectory and thereby simulate a dimension of 1. This problem was solved by [12] by excluding the pairs which are close, not because of the attractor geometry but since they are correlated. This is usually the case when they are close in time, thus Eq. (4) is modified so that the second sum starts after some correlation time $t_{\min} = n_{\min} \Delta t$ has elapsed. This introduces a time separation between the points \mathbf{x}_i and \mathbf{x}_j in the time ordered vectors

$$C(\varepsilon) = \frac{2}{(N - n_{\min})(N - n_{\min} - 1)} \sum_{i=1}^{N} \sum_{j=i+n_{\min}}^{N} \Theta(\varepsilon - \|\mathbf{x}_i - \mathbf{x}_j\|).$$
 (9)

No exact rule of thumb considering the choice for n_{\min} exists, but a recommendation $n_{\min} \geqslant \tau_d$ is given. The space time separation plot was introduced by [13] as a method to estimate a safe value for the correlation time t_{\min} .

After taking account to the temporal correlations in the data the correlation sum can be evaluated for the reconstructed attractor. The result is plotted as a log/log plot and a power-law behaviour should be found within some scaling region, typically for a small length scale ϵ for experimental data. The power-law behaviour of $C(\varepsilon)$, which is the signature of self-similarity in the data, can best be found plotting the slope $d(\varepsilon)$ of the log/log plot of $C(\varepsilon)$. Then a plateau of $d(\varepsilon) = \frac{\partial \ln C(\varepsilon)}{\partial \ln \varepsilon}$ corresponds to the power-law behaviour of $C(\varepsilon)$.

When analysing the local slopes for $d(\varepsilon)$, three different regions can be distinguished, see figure 10.

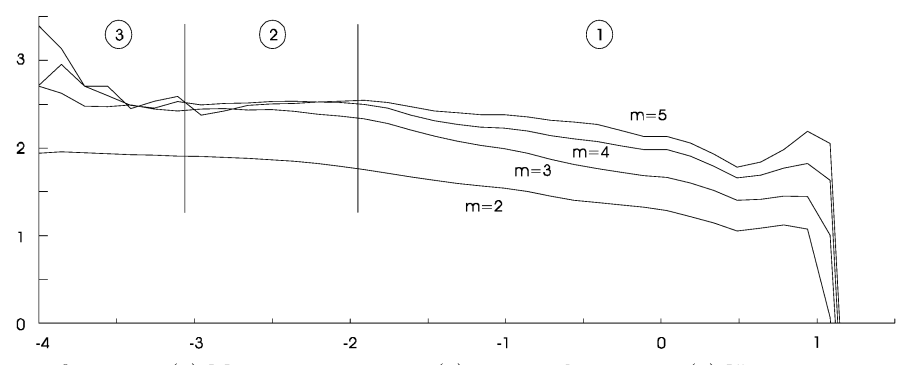


figure 10. (1) Macroscopic regime, (2) True scaling range, (3) Noise regime

The finite size of the attractor obviously introduces a cut-off in the graph. For large ε the macroscopic structure gives a value which varies with ε and m. For smaller length scales the true scaling range is found once the attractor is fully unfolded, i.e. the embedding m is large enough, and the value for $d(\varepsilon)$ should remain approximately constant when increasing m. If this is the case and the plateau is convincing enough a value for the fractal dimension of the attractor may be estimated. On smaller length scales, the effect of noise and lack of neighbours will destroy the fractal structure, and the local scaling exponent will reach the value of the embedding dimension. The different regions discussed very much depend on the quality and amount of data fed to the algorithm.

4.3.3 Data Requirements

Paper [14] discusses the data requirements for a reliable estimation of the correlation dimension, but no general rule of thumb can be given since the requirements depend on the attractor to be reconstructed.

Number of Data Points Needed The number of data points to be used very much depends on the structure of the attractor, and the distribution of the points. If the orbits rarely visit the areas with fractal structure there is a need for a very large number of points to resolve the attractor's dimension, if possible at all. Paper [15] states that "...experience also indicates the need for more experience...".

So, the only way to be sure that the number of points used is enough is to look for convincing evidence of self-similarity in the results. If a too small dataset is used, the scaling region for the plateau will decrease and the value for $d(\varepsilon)$ will typically increase with increasing m. An incorrect value for the estimation of d might be the result, since the scaling region investigated is not confined to the small length scales and therefore is not a property of the self-similarity in the attractor. An example of a failure estimating the fractal dimension for a simple five-dimensional system can be found in [16].

The Effect of Noise The effect of noise is another aspect that highly influences the performance of the correlation integral. This is investigated in [17] and [18] for some familiar dynamical systems, and the results indicate an increase in fractal dimension for noisy attractors. The larger the noise level, the smaller the plateau for $d(\varepsilon)$ will be. This results in a destroyed fractal structure of the attractor, and will cause the curves in the dimension estimation graphs to strive towards the embedding dimension for length scales below the amplitude of the noise. If the plateau is hard to distinguish there is a need to apply noise reduction to the data.

The Effect of Filtering Linear filtering methods is as a rule not recommended to deterministic chaotic data [15], since it can artificially increase the measured correlation dimension. Instead of using linear filtering [10] suggests the use of nonlinear noise reduction methods, to recover the self-similarity of the underlying dynamical system.

4.4 Dimension Analysis of an Impact Oscillator

As a first example an attractor reconstruction of the attractor w=2.34, using the displacement signal, was carried out. A value for the delay time was chosen according to the first zero crossing of the autocorrelation function, yielding $\tau=13$, to be compared with the value achieved for the first minimum of the mutual information function, $\tau=17$. The number of points in the data sets used is 76800, which corresponds to about 30 points/driving-cycle. Figure 11(a) shows a 2-D projection of the true attractor whilst figures 11(b) and (c) show the reconstructions.

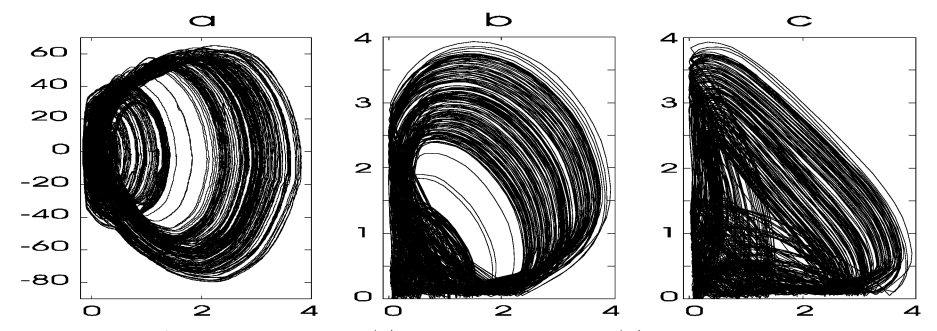


Figure 11. Attractors w=2.34 (a) Original attractor, (b) Reconstructed attractor $\tau=13$, (c) Reconstructed attractor $\tau=17$.

Computation of the correlation integral, equation 9, was performed using the box-assisted algorithm described in [10]. The procedure by which the correlation integral is computed is illustrated in figure 12, where (a) and (b) show the log/log plots of the correlation integral. The scaling region is chosen by examining figures (c) and (d), which illustrates the slopes of (a) and (b) as a function of the length scale.

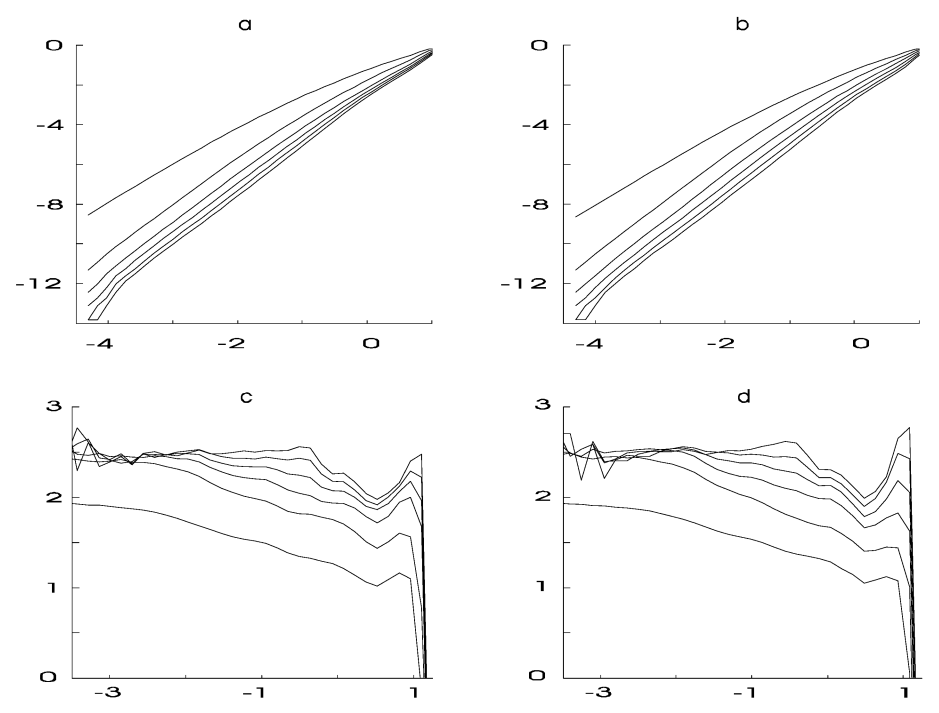


Figure 12. Correlation integral results of the experimental displacement data, w=2.34,(a) The log/log plot, $\tau=13$, (b) The log/log plot, $\tau=17$, (c) The local slopes of (a), (d) The local slopes of (b)

To find a final measure of the correlation dimension, the slopes of figure 12(c) and (d) has to show a convincing plateau. For the data sets analysed here, the true scaling region is found in the region $-3<\log(\varepsilon)<-2$. The two different estimations indicate approximately the same dimension, where $d\approx 2.5\pm 0.05$, so the use of the auto-correlation function seems to yield a good estimation for the delay time.

At large embeddings, the scaling region decreases and is confined to larger ε , as a result of the lack of neighbouring points. For an increased number of points, corresponding to increased statistics in the data, a larger scaling region would have been preserved for even higher embeddings.

Analysing figures 12(c) and (d), the three regions previously discussed can be detected. In the microscopic regime for embedding dimension m=2, the curves are seen to strive towards the embedding dimension, since the attractor is not fully unfolded. The fluctuations in the curves are due to the lack of neighbouring points.

Comparing the results with an estimation using the velocity signal, figure 13, the results yields a slightly lower dimension $d\approx 2.35\pm 0.05$ in the scaling region around $0<\log(\varepsilon)<1$. The delay time used was $\tau=10$.

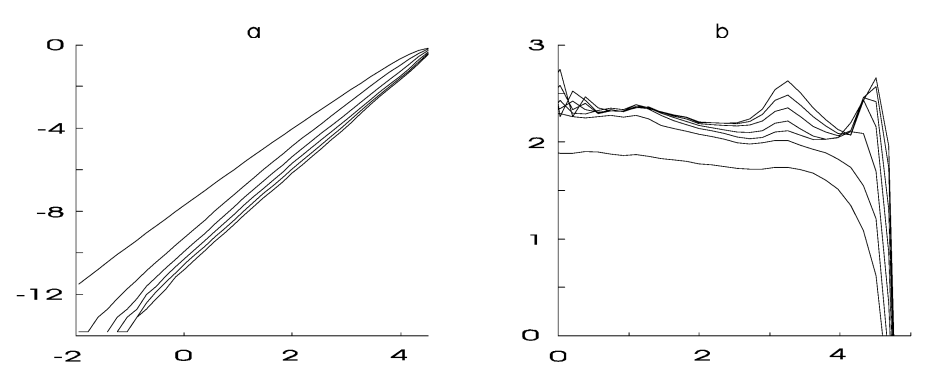


Figure 13. Correlation integral results of the experimental velocity data at w=2.34, (a) The log/log plot, (b) The local slopes of (a)

Comparing the estimations for w=2.34 with an estimation performed on the Poincaré section, the results argues for a dimension $d\approx(1+1.5)\pm0.05$ in the scaling region around $-4<\log(\varepsilon)<-2$, figure 14.

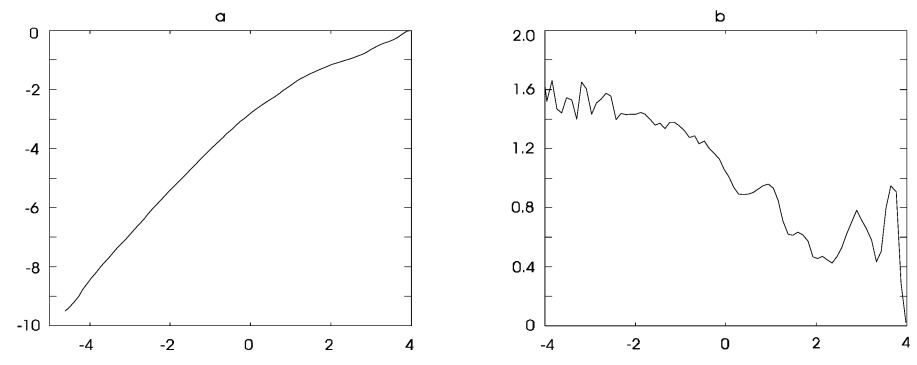


Figure 14. Correlation integral results of the experimental Poincaré section, w=2.34, (a) The log/log plot, (b) The local slopes of (a)

The results from the numerically generated data, w=2.56, are seen in figure 15. A delay time $\tau=8$ was used for the displacement data and $\tau=11$ for the velocity data. The result yields very much the same behaviour as for the experimental data, where the estimation from the velocity signal indicates a slightly lower dimension than the one from the displacement signal.

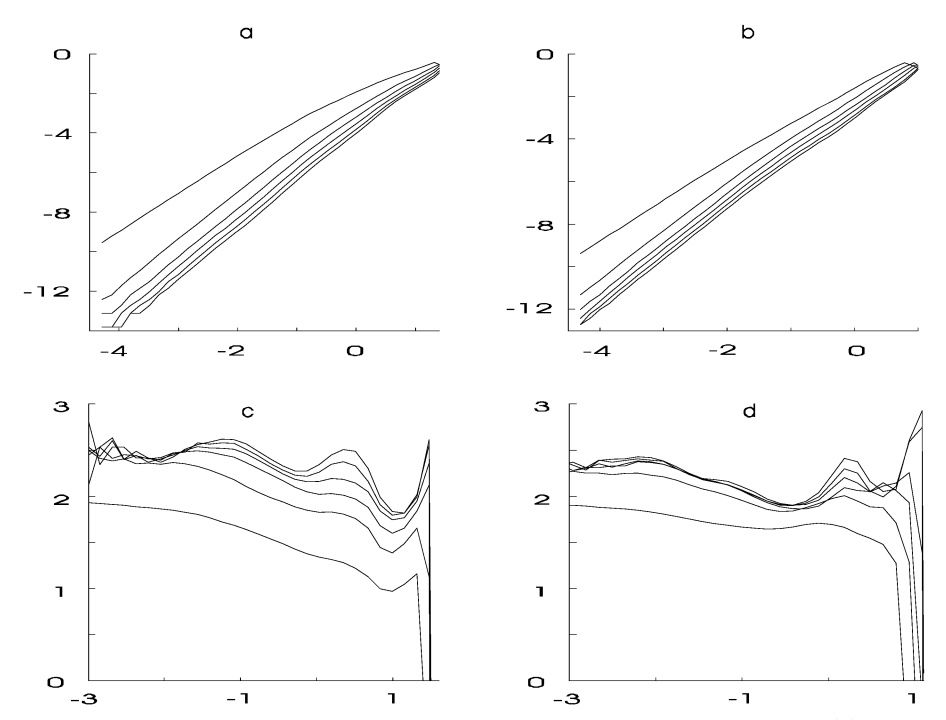


Figure 15. Correlation integral results of the numerical data at w=2.56, (a) The log/log plot of the displacement signal, (b) The log/log plot of the velocity signal, (c) The local slopes of (a), (d) The local slopes of (b)

The estimation yields a dimension $d\approx 2.45\pm 0.05$, in the approximate scaling region -3<log(ε)<-2, for the displacement signal and $d\approx 2.35\pm 0.05$ for the velocity signal.

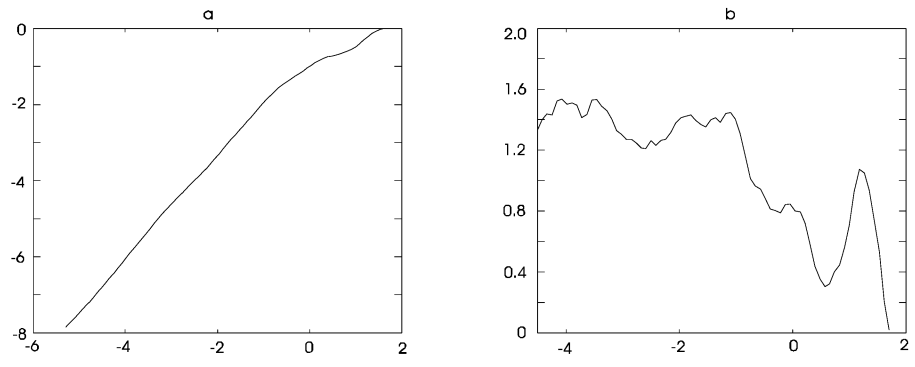


Figure 16. Correlation integral results of the numerical Poincaré section, w=2.56, (a) The log/log plot, (b) The local slopes of (a)

The Poincaré section estimates a dimension $d{\approx}(1+1.45){\pm}0.05$ in the scaling region around -4.3<log(ε)<-3.5.

The next estimation, figure 17, was performed using the experimental attractors at w=3.98, corresponding to a sampling of about 15 points/driving-cycle. The delay times used were $\tau=23$ for the displacement signal and $\tau=9$ for the velocity signal.

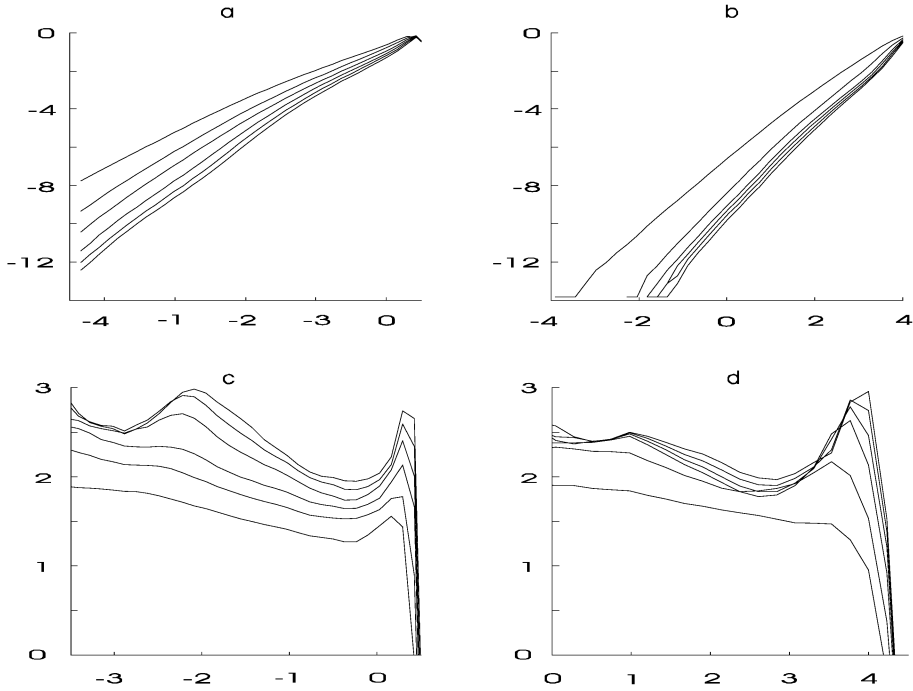


Figure 17. Correlation integral results of the experimental data at w=3.98, (a) The log/log plot of the displacement signal, (b) The log/log plot of the velocity signal, (c) The local slopes of (a), (d) The local slopes of (b)

The scaling region for the displacement signal is less defined in this estimation but indicates a dimension $d\approx 2.5\pm 0.05$ in the region -3.3<log(ε)<-2.6. For the velocity signal the plateau is found for -1<log(ε)<0 and the dimension can be estimated to $d\approx 2.45\pm 0.05$. The Poincaré dimension estimation argues for a slightly lower dimension around $d\approx (1+1.35)\pm 0.05$ in the scaling region around -2.8<log(ε)<-1.5, see figure 18.

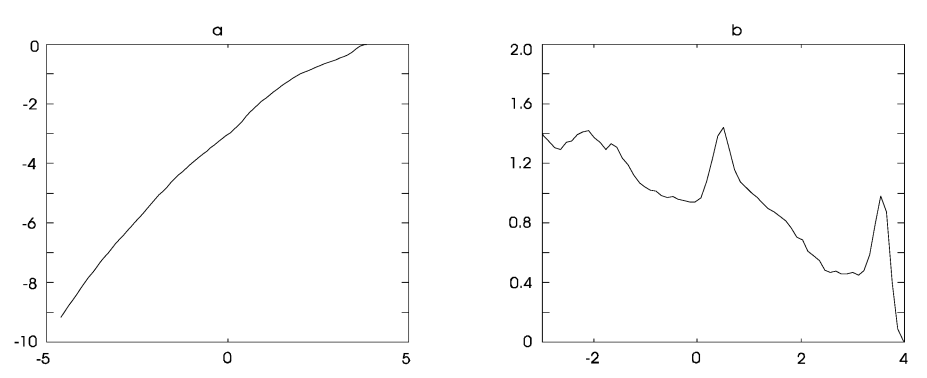


Figure 18. Correlation integral results of the experimental Poincaré section, w=3.98, (a) The log/log plot, (b) The local slopes of (a)

For the estimation using the numerically generated data from the attractor $w{=}4.52$, see figure 19, the scaling region is found around -2<log(ε)<-1 for the displacement signal and -3<log(ε)<-2 for the velocity signal, indicating the dimensions $d{\approx}2.45{\pm}0.05$ and $d{\approx}2.3$.

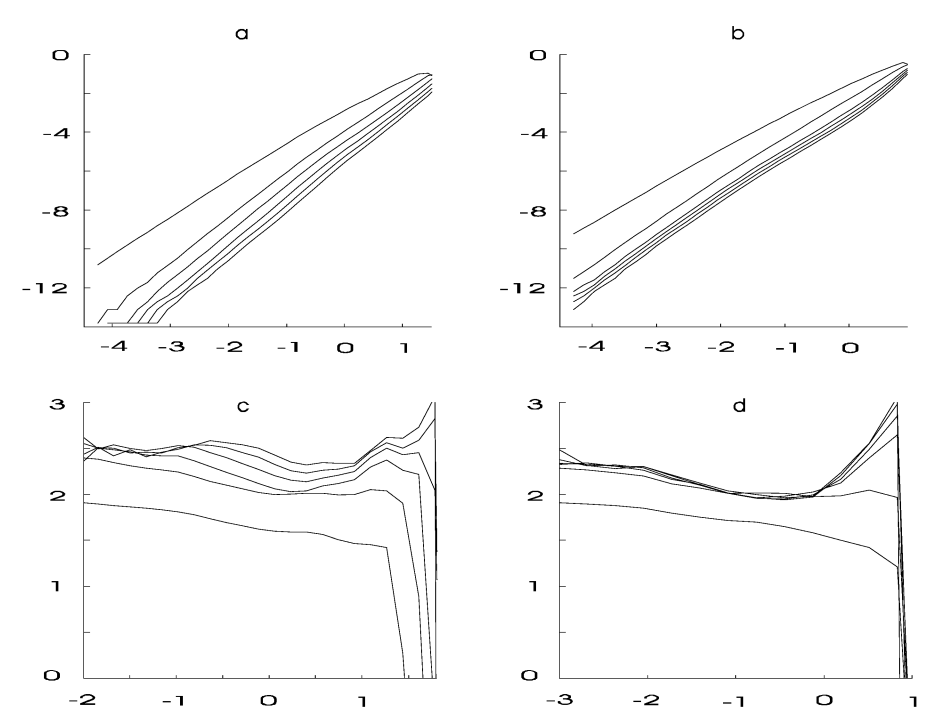


Figure 19. Correlation integral results of numerical data w=4.52, (a) The log/log plot of the displacement signal, (b) The log/log plot of the velocity signal, (c) the local slopes of (a), (d) the local slopes of (b)

The Poincaré dimension estimation argues for a dimension around $d\approx(1+1.45)\pm0.05$ in the scaling region around -4.5 $<\log(\varepsilon)<$ -3.5, figure 20.

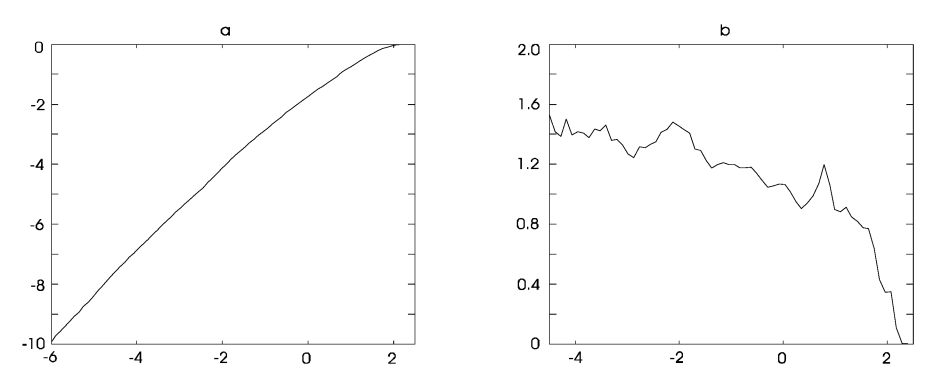


Figure 20. Correlation integral results of the numerical Poincaré section, w=4.52, (a) The log/log plot, (b) The local slopes of (a)

5 Discussion and Conclusions

An experimental and numerical study of the dynamics in an impact oscillator has been carried out. The results has been analysed using the method of correlation dimension, in order to investigate the fractal dimension of the chaotic attractors. A very good match between the experimental and theoretical dynamics was achieved, where the attractors showed very similar structure. In the dimension analyses, the sampling of the time series was found to be an important issue since the number of points that can practically be evaluated are limited due to the computing time for large time series. If the formula for the correlation sum $C(\varepsilon)$ is evaluated directly as two nestled loops it will contain about $N^2/2$ terms for N points, which makes the computation very time consuming. The use of multidimensional trees can achieve a performance with the number of operations proportional to $N \log N$, which is the best performance for sets with arbitrary distribution. The box-assisted approach used in this report is preferred due to its simplicity and it is generally faster for rather low-dimensional sets. For data sets where the points are not too clustered the operation count will be $\propto N$ for N points [10].

If a too high sampling is used the statistics in the analyses are limited and convincing plateaus, indicating self-similarity in the attractor, will not be found. The curves will typically have a slope, resulting in less defined plateaus, and a dimension estimation cannot be performed. For the attractors considered in this report the number of points used were about 80000, with a sampling corresponding to 17-30 points/driving-cycle yielding 2600-4400 driving-cycles in the estimation depending on the attractor analysed.

For all analyses, the attractors were fully reconstructed at an embedding dimension m=5, but the recommendation [7] yielding m=7 was used in the

analyses to make sure that the dimension remained approximately constant for increasing embeddings. The results from the estimations indicates a fractal dimension of about $d=2.4\pm0.1$, which was verified by the estimations from the Poincaré sections. The estimations coming from the velocity signal resulted in a slightly lower value than the ones coming from the displacement signals. A good agreement between the experimental and theoretical estimations was found and the results verifies that the dynamics lives in a three dimensional space, in agreement with the number of states used when modelling the equations.

6 Acknowledgement

My supervisor Docent Arne Nordmark is gratefully acknowledged for the support and guidance during this work. Kent Lindgren and Danilo Prelevic at the Marcus Wallenberg Laboratory for Sound and Research are also acknowledged for providing valuable help with experimental issues.

References

- [1] P. Grassberger and I. Procaccia, Measuring the strangeness of strange attractors. Physica D 9, 189 (1983).
- [2] E. Lorenz, Deterministic nonperiodic flow. J. Atmos. Sci. 20, 130 (1963).
- [3] J. D. Jiang, J. Chen and L. S. Qu, *The application of correlation dimension in gearbox condition monitoring*. Journal of Sound and Vibration, 223(4), 529 (1999).
- [4] C. Craig, R.D. Neilson and J. Penman, The use of correlation dimension in the condition monitoring of systems with clearance. Journal of Sound and Vibration 231(1), 1 (2000).
- [5] A. Stensson and A. B. Nordmark. Experimental investigation of some consequences of low velocity impact in the chaotic dynamics of a mechanical system. Philosophical Transactions of Royal Society of London A 347, 439 (1994).
- [6] G. P. Williams, Chaos Theory Tamed. Taylor & Francis Limited. ISBN:0-7484-0749-9 (1997).
- [7] F. Takens, *Detecting strange attractors in turbulence*. Lecture Notes in Math. 888, Springer-Verlag (1981).
- [8] E. Ott, T. Sauer, J. Yorke, Coping with chaos: analyses of chaotic data and the exploitation of chaotic systems. John Wiley & Sons, Inc. ISBN:0-471-02556-9 (1994).

- [9] J. M. Martinerie, A. M. Albano, A. I. Mees, P. E. Rapp, Mutual information, strange attractors, and the optimal estimation of dimension. Phys. Rev. A 45, 1770 (1994).
- [10] H. Kantz and T. Schreiber, *Nonlinear time series analysis*. Cambridge Nonlinear Science Series 7. ISBN 0-521-65387-8 (1999).
- [11] A. M. Fraser and H. L. Swinney, *Independent co-ordinates for strange attractors from mutual information*, Phys. Rev. A33, 1134 (1986).
- [12] J. Theiler, Spurious dimension from correlation algorithms applied to limited time-series data. Phys. Rev. A 34, 2427 (1986).
- [13] A. Provenzale, L. A. Smith, R. Vio and G. Murante, *Distinguishing between low dimensional dynamics and randomness in measured time series*. Physica D 58, 31 (1992).
- [14] A.M. Albano, A.I. Mees, G.C. de Guzman and P.E. Rapp, Data requirements for reliable estimation of correlation dimensions. Chaos in biological systems, edited by H. Degn, A.V. Holden and L.F. Olsen (Plenum Press, New York, 1987).
- [15] J. Theiler, Estimating fractal dimension. J. Optical Soc. Am. A 7, 1055 (1990).
- [16] A. Jedynak, M. Bach and J. Timmer, Failure of dimension analysis in a simple five-dimensional system. Phys. Rev. E 50, 1170 (1994).
- [17] A. Ben-Mizrachi, I. Procaccia and P. Grassberger, Characterization of experimental (noisy) strange attractors. Phys. Rev. A 29, 975 (1984).
- [18] J. Argyris, I. Andreadis, G. Pavlos and M. Athanasiou, *The influence of noise on the correlation dimension of chaotic attractors*. Chaos, Solitions & Fractals, Vol. 9, 343, (1998).
- [19] L. N. Virgin, Introduction to experimental nonlinear dynamics: a case study in mechanical vibration. Cambridge university press, ISBN: 0-521-77931-6 (2000).

7 Appendix

7.1 Experimentally Obtained Parameter Values

7.1.1 Natural Frequency and Damping

The damping in the spring mass system was measured using the logarithmic decrement method. An exponential decay curve was fitted to the amplitude response of a free oscillation in the spring/mass system, see for example [19].

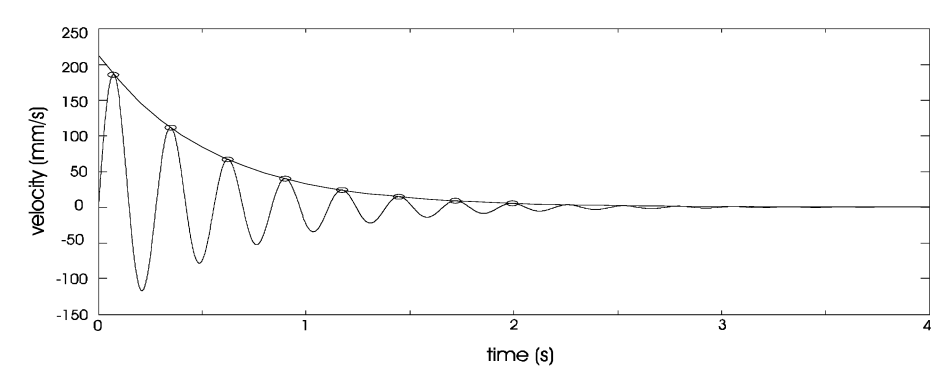


Figure 21. A free decay of the mass/spring system

The decay curve x has the following relation to the damping and undamped/damped natural frequencies

$$x = x_0 e^{-\beta t} = x_0 e^{-\zeta \omega_n t}$$

$$\omega_d = \omega_n \sqrt{1 - \zeta^2}$$

The damped natural frequency is achieved from the free decay by measuring the period time T_d for an oscillation

$$\omega_d = \frac{2\pi}{T_d}$$

and the values for the damping ζ and undamped natural frequency ω_n can be calculated

$$\beta = \frac{\zeta \omega_d}{\sqrt{1 - \zeta^2}}$$

$$\zeta = \sqrt{\frac{1}{1 + \left(\frac{\omega_d}{\beta}\right)^2}}$$

Several measurements were done and averaged, resulting in the values $\zeta = 0.078$ and $\omega_n = 3.67 \text{Hz}$ for the damping coefficient and the natural frequency.

7.1.2 Coefficient of Restitution

The coefficient of restitution was measured by taking the ratio of two consecutive velocities, before and after impact. As an example the relative velocity, before and after impact, is analysed.

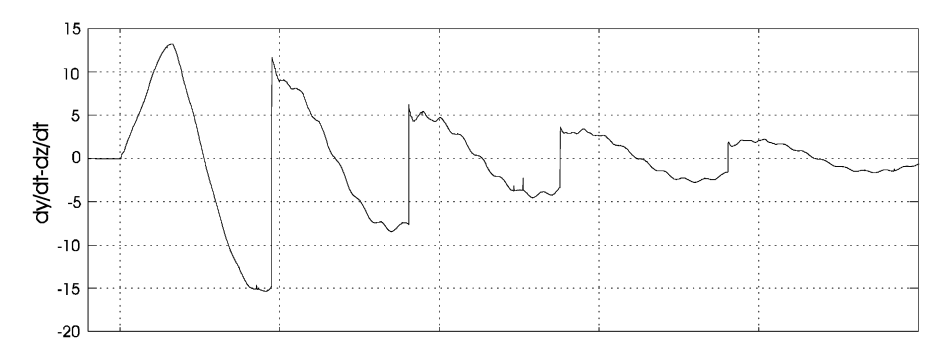


Figure 22. Relative velocity for the impacting system

For the first impact, figure 22, the in-velocity is approximately 15 mm/s and the out-velocity about 12 mm/s, yielding a coefficient of restitution e=0.8. An average over several measurements and different in-velocities was done and the resulting ratio found to be about 0.82. Indications that the coefficient of restitution varies with in-velocity, yielding a larger value for low velocities, were seen but the uncertainty in the measurement results lead to the use of an averaged value.

7.1.3 Equilibrium Standoff Distance between Mass and Base

The amplitude of the base was increased until impact occurred with the mass, originally at rest. The value for the base amplitude when this happens was taken as the static equilibrium standoff distance. This value can only be taken as an approximation, since the value might change during the run and especially after a resonance peak.

Paper A

An Experimental and Numerical Study of Pantograph Dynamics, with the Application of Dimension Estimation

J. Eriksson¹, A. B. Nordmark¹ and L. Drugge²
¹Department of Mechanics, ²Division of Vehicle Dynamics,
Aeronautical and Vehicle Engineering,
Royal Institute of Technology, SE-100 44 Stockholm, Sweden

April 1, 2005

Abstract

The performance of the current collection for a railway train depends on the interaction between the pantograph and its catenary system. As there is a demand for increased speed of the trains new challenging problems arise, whereby a good understanding of the systems' dynamic performance is of importance. In this study an experimental investigation of a Schunk WBL88/X pantograph is performed, with the focus on its complex behaviour. In particular, the complex response known as chaos is characterised using the method of correlation dimension. A mathematical model is developed of a subsystem and the numerical results are compared with experimental. A qualitative good agreement is found in the results, and effects from friction and impacts are found to highly affect the behaviour of the system.

1 Introduction

A pantograph current collector is the system that provides the electric power from the overhead catenary system to a railway train. Due to the demands for increased speed of the trains, and compatibility with other countries' catenary systems challenging problems arise. The problems are for example unsatisfactory current collection, arcing and increased wear. The current collection depends on the interaction between the pantograph and the catenary system, whereby a good understanding of their dynamical properties is crucial. Since different countries have their own standards for the catenary system and the economic considerations involved making changes to it, the research of today is focused on the performance of the pantograph. In the analysis of pantograph dynamics, there is a need for experimental measurements and development and simulation of mathematical models.

Pantograph models previously reported in the literature spans from single mass models to four mass models, with linear and nonlinear geometry and suspension elements. The driving of the models varies from simple force and displacement excitation to more advanced methods, with a finite element model of the catenary system. Drugge et al. [1] analysed the behaviour of the contact strip, using a single degree of freedom model (SDOF) with translational freedom, suspended in a nonlinear suspension element. Harmonic, subharmonic as well as chaotic response is reported for periodic forcing of the model. A linear SDOF model with parametric forcing is considered by Wu and Brennan [2], where an analytical investigation of the pantograph-catenary system's stability is performed. The finite element method is used to determine the catenary characteristics, and Floquet theory when studying the coupled system. Jerrelind and Stensson [3] developed a single mass model of the head assembly, with translational and rotational freedom around its centre of mass. Symmetric and asymmetric forcing is considered and the focus of the study is on the coupling effects, introduced by the two interacting piecewise linear suspension elements in the model. The results show harmonic as well as subharmonic, quasiperiodic and chaotic response, when harmonic forcing is applied, and conclusions are drawn that models with uncoupled motion cannot even be used as a worst case measure.

The single mass models can provide understanding of a subsystem in the pantograph, but if the full systems behaviour is to be evaluated the minimum requirement is the use of a two mass model, so that the motion of the frame assembly is included in the study. Drugge and Stensson [4] used a two DOF pantograph model when investigating the effects of catenary damping on the subsequent oscillatory motion of catenary systems. Single and multiple pantograph operation were considered and the results compared with experimental, from full scale field measurements. Eppinger et al. [5] reviewed different models ability to predict the pantograph's behaviour. An asymmetric nonlinear three DOF model is developed and experimental evaluation of the results performed. The results argues for the use of a three DOF model, if frequencies above the first resonance are considered, since the analytical and experimental results shows that motion of the upper and lower frame will typically be out of phase above this frequency.

A three DOF model with nonlinear geometry, damping and stiffness is formulated in Seering et al. [6], and numerical results evaluated with experimental. Responses from the model and experimental data showed harmonic and subharmonic motion under harmonic excitation. Another paper investigating a three-dimensional pantograph is found in Lesser et al. [7], where the rotation of the contact strip was taken into account. A moving load excitation, along the contact strip, was used and the results showed that the major motion of the pantograph was due to rotation of the contact strip. The results argue for inclusion of contact strip rotation if a realistic model is to be developed. Larsson and Drugge [8] performed a parameter study of the suspensions in the head assembly, using a three dimensional pantograph model. The important parameters were found to be the viscous damping and friction.

In Poetsch et al. [9] a review of existing pantograph model designs is found. The limitations of the pantograph-catenary systems are outlined and proposals for active control concepts discussed. Pracik and Furmanik [10] developed a nonlinear four DOF model, with translational freedom. The model is built up by four masses where two represents the frame assembly and the other two the contact strips, and the results showed non-harmonic response for harmonic excitation.

The authors claim the use of the correlation dimension method, but no results from dimension estimations are presented. This is the only paper found that reports application of the correlation dimension method to measurement data from a pantograph, and that method is used in this report.

The pantograph considered in this report is a Schunk WBL88/X, built up by several parts. On top is a head assembly, which consists of two contact strips (that collects the electricity from the catenary system) supported in suspensions attached to a head frame. The head assembly is supported by a frame assembly, built up by two hinged links, with an air-suspension that provides up-lift force to the structure. In this work an experimental investigation of the pantograph's behaviour at different frequencies is carried out. To provide better understanding for the origin of some behaviour of the pantograph, investigations are also performed with the head assembly fixed to ground. A mathematical model of the latter case is developed and numerically analysed. The model is, due to the decoupling in the head assembly, restricted to one contact strip with translational and rotational freedom around its centre of mass. An additional mass, with vertical freedom, is added at the centre of the contact strip, to simulate a bending oscillation in the strip. The model includes nonlinearities, such as possible loss and impact at the excitation, friction and piecewise linear stiffness. The forcing is applied at the additional mass through a stiff periodically excited suspension element.

When applying dimension estimation to a data set, a measure of the minimum number of state variables needed to describe the underlying dynamical system is achieved. Another property of the estimator is that it can distinguish between chaotic and random motion that, in combination with information about the minimum number of state variables needed, provides useful information in the design stage of new simulation models.

2 Experimental Set-up

An experimental set-up of the pantograph, Schunk WBL88/X, was previously designed and used for the study of the pantograph's dynamical behaviour by Harèll et al [11]. This work focused on the coupling effects, introduced by the interaction between piecewise linear suspension elements in the construction, and gives a more detailed review of the experimental set-up. The pantograph is built up of two subsystems; the head and frame assembly, with the schematic structure as seen in figure 1. The frame assembly consists of two frames, an upper (8) and a lower (9) that connects to one another, the ground and the

head frame (1) with y-axis rotational joints. An air-spring provides up-lift force to the structure, and two friction dampers (11) are attached between the lower frame (9) and the ground. A third friction damper (7) connects between the upper (8) and head frame (1). The design, where a bar link (10) connects from the lower frame (9) to the ground, restricts the head frame's motion to displacement along the z-axis.

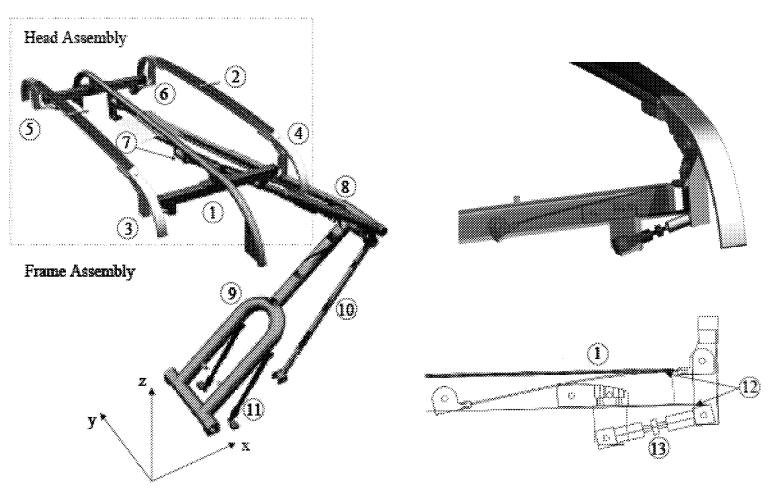
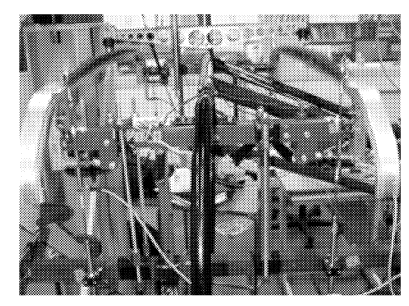
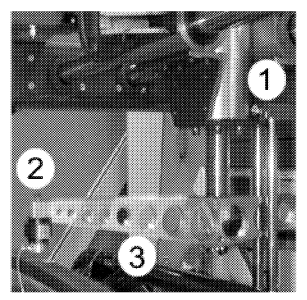


Figure 1. Schematic view of the pantograph assembly, where (1) is the head frame, (2) a carbon collector strip, (3)-(6) suspensions, (7) the connection point for the friction damper between upper and head frame, (8) upper frame, (9) lower frame, (10) bar link, (11) friction dampers and the location of the air-suspension, (12) the leaf springs and (13) is one of the rigid links.

The head assembly includes two carbon collector strips, where the one marked (2) is referred to as the back contact strip (cs_b) and the other as the front contact strip (cs_f) , and a head frame (1), at which the strip ends are suspended. The suspensions are built up by leaf springs (12) and rigid links (13), which allow an x-rotational and z-translational motion of the strip, and their location on the strip referred to as the left (3)(4) and right (5)(6) side $(cs_{fl}, cs_{bl}, cs_{fr}, cs_{br})$. The same front/back and left/right reference structure and numbering applies to the head frame (1), $(hf_{fl}, hf_{bl}, hf_{fr}, hf_{br})$. The motion of the strip is limited by the head frame in upward displacement, referred to as the upper limit, and a lower leaf spring (12) in downward displacement, referred to as the lower limit, introducing a piecewise linear characteristics in the suspension.

In the set-up a hydraulic system (MTS 458), with a signal generator (Brüel& Kjaer Puls) and hydraulic actuator (MTS 242.01) marked with (1) in figure 2, is used. The actuator, which is placed in a rigid foundation built around the pantograph, provides a sinusoidal forcing to the strips via an aluminium beam (3) attached to its piston.





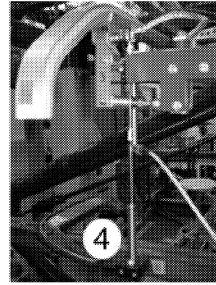


Figure 2. The experimental set-up, where (1) indicates the hydraulic actuator, (2) is one of the excitation contact switches, (3) is the aluminium excitation beam and (4) one of the inductive displacement transducers.

At each of the contact strips' suspensions and head frame's ends, inductive displacement transducers (LVDT, Hottinger 1-WA/50&100MM-L) are located (4). The ones attached to the contact strip measures its displacement vs. the head frame and the ones attached to the head frame measures displacement vs. ground. The motion of the excitation is measured by an internal displacement transducer in the hydraulic actuator and, in difference with the experimental set-up in Harèll et al [11], contact sensors were added to indicate when the lower limits are reached or if contact loss occurs between the excitation beam and the strips, (2) in figure 2. The signals were recorded at a sampling rate of 6000Hz using a recorder (Sony DAT) and the signal is amplified with an amplifier (MGC plus, Hottinger).

Due to the complexity of the pantograph dynamics, the head frame was fixed to ground in Case 2 and 3, see below, and for Case 3 cs_f was removed and an additional measurement of the other strip's centre point performed using a laser (Polytec OFV303), measuring its velocity.

3 Experimental Methodology

During the experimental runs, the pantograph was excited at fixed amplitude and frequency and the transients in the dynamics allowed to die out before a measurement was recorded. The frequency was increased, whilst still exciting the pantograph, between the measurements and the same procedure as mentioned above repeated.

By this methodology, an overview of the dynamical behaviour that occurs at the frequencies investigated, when holding other parameters (such as the amplitude) fixed, is achieved. Using the frequency sweep method it is possible that some of the behaviours are missed, since co-existing solutions might be present at certain frequencies. Those solutions could possibly have been found, using the same initial conditions at every frequency considered or perturbing the pantograph during run.

The results presented are 20s of the recording, if nothing else is mentioned, and filtering is only applied before taking derivatives of the displacement trans-

ducer data, to compute the velocity. The filtering used is a 6th order low-pass FIR filter, with a cut-off frequency at 100Hz. The laser velocity data is automatically integrated in the laser and no post processing therefore needed.

In the experimental work three different cases are considered, all excited at the centre of the strips, with configurations as presented in table 1.

Case	Head Frame	$F_p(N)$	A(mm)
1	Free	25	5
2a	Fixed	6	5
2b	Fixed	12	10
3	Fixed	25	5

Table 1. Description of the studied cases

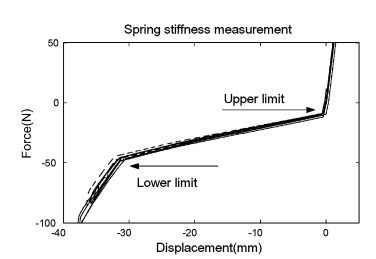
The first case, referred to as Case 1, is on the full rig with the air-suspension adjusted to provide a total up-lift force of 100N. The up-lift force is measured at the contact points between the excitation beam and the strips, and results in a preload of the strips. The preload is equivalent to F_p =25N, in each of the suspensions, when the excitation is at its static zero level, and results in a compression of the suspensions. This allows impact at the suspensions lower limits and an investigation of the pantograph's dynamical behaviour under these circumstances can be carried out.

In Cases 2 and 3 the head frame is fixed to ground. For Case 2, the zero level of the excitation adjusted so that the excitation beam is just in contact with the contact strip in the excitation's upper turning point. This results in a strip preload of F_{pa} =6N and F_{pb} =12N at each of the suspensions, and allows one side of the strip to impact at its upper limit.

For Case 3 cs_f is removed, to make sure that none of its dynamics is transferred via the excitation beam to the other contact strip. The zero level of the excitation is adjusted to give a comparable situation to Case 1, with a preload of F_p =25N, and an investigation whether similar situations arise as for the full system can be carried out. In this case a laser, measuring the contact strip's centre's velocity, provides additional information about its motion.

4 Pantograph Characteristics

To provide a better understanding of the experimental results and estimate parameters for the mathematical model to be developed, some of the pantographs characteristics were analysed. The head assembly was taken apart, so that the spring stiffness of the individual suspensions and the strip's inertia could be determined. The results from the stiffness measurements are presented in figure 3, where all four suspensions are found to have similar characteristics. A small variation in the location of the lower limit is found for the suspension at cs_{fr} , position (5) in figure 1, here marked with a dashed line. The measurements yielded the approximate stiffness k_U =47500N/m in the upper limit, k=1150N/m for the free spring and k_L =7550N/m in the lower limit.



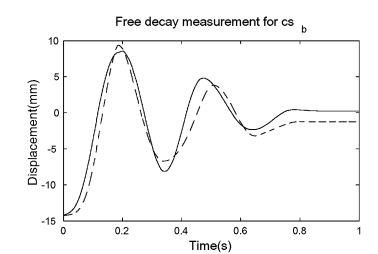


Figure 3. The stiffness characteristics of the unloaded suspensions and a free decay for contact strip back, where the dashed line is from the left side and the solid line from the right

The friction present in the suspensions depends on the amount of force used when attaching them to the head frame and the contact strips. For this reason, a free decay measurement of the contact strip was preferred to one in the rig previously used to determine their stiffness. Contact strip cs_b was chosen for this purpose and to prevent it from impacting with the upper limit an additional mass of 1.6kg was added to it. Analysing a free decay, figure 3, the difference in amplitude between two successive peaks should relate to each other as $4F_f/k$, Tedesco et al. [12], where F_f is the resulting friction force. Measurements from the right and left side resulted in the approximate friction forces F_{f_r} =1N and F_{f_l} =1.6N. To get a more realistic measure of the friction, analyses at various frequencies would be needed and is not considered in this study.

To determine the contact strip's inertia, I, it was pivoted at its centre of mass and springs, with known stiffness, added at each side of the pivot point at distance L_1 , as seen in figure 4. The rigid links, that normally connects the strip to the springs, were included in this test since they will affect the inertia. A displacement transducer was placed at distance L_2 , to measure the response of the free decay. Two different setups with springs were used and several measurements performed, to get an averaged value for the inertia coefficient.

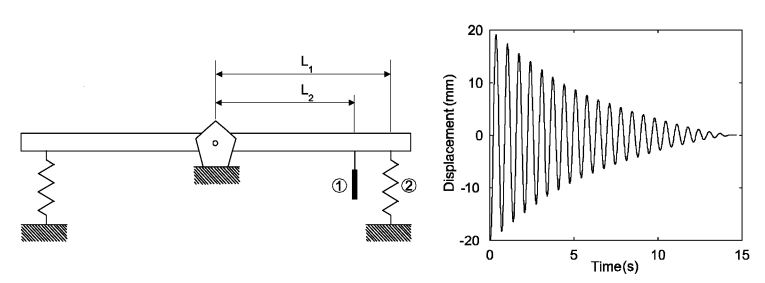


Figure 4. Contact strip suspended in springs and a free decay of the contact strip

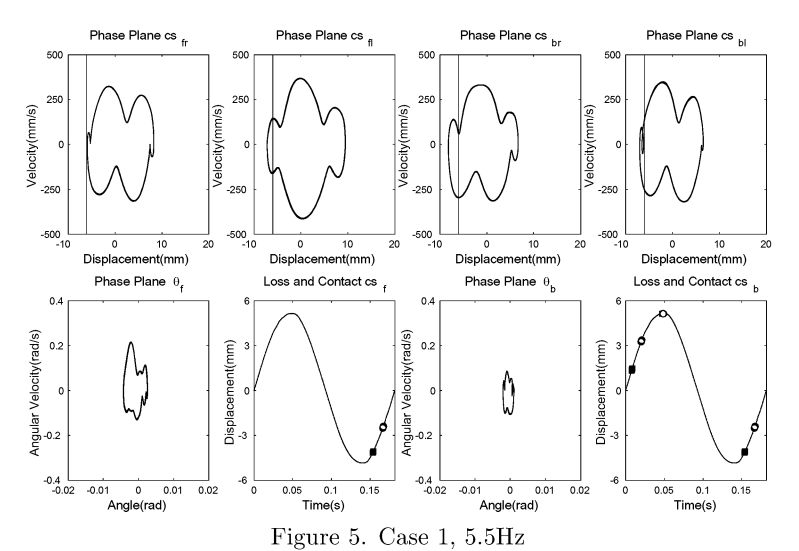
Analysing a free decay, the natural frequency, w_n , can be determined and using its relation to the spring stiffness, k, and strip length, L_1 : $w_n^2 = 2kL_1^2/I$, Tedesco et al. [12], an averaged value $I = 0.78 \text{kgm}^2$ could be calculated. The mass of the strip, including links, was found to be m = 3.5 kg.

5 Experimental Results

In this section four ways of presenting the results are used: phase plane plots, time histories, maximum amplitude diagram and Poincaré sections. The phase plane plots are simply the displacement plotted vs. velocity, time history is time vs. displacement and the maximum amplitude diagram the frequency vs. maximum displacement. The Poincaré section is a section of the phase plane plot, sampled once every excitation cycle when the excitation is in its upper turning point, and the results are from 2000 excitation cycles.

5.1 Case 1

In the first example, see figure 5, the excitation frequency is 5.5Hz. The phase plane plots for cs_f and cs_b , with their left and right side coordinates z_{fl} , z_{fr} , z_{bl} , z_{br} , have a vertical line that indicate the location of the lower limit, which has to be considered as approximate since it varies slightly between impacts. The phase plane plots of the contact strips angles, θ_f and θ_b , is approximated from the transducer data, which has the following linearised relation to cs_f 's angle: $\theta_f = (z_{fl} - z_{fr})/(2L)$. The time history data of the excitation is marked with a " \blacksquare ", when there is a contact loss between the strip and excitation beam, and a "o", when back in contact, so that conclusions about the effects introduced by loss and impact can be drawn.



When repeated loss and impacts occur, the marking for loss might appear before the marking for contact, since 20s of the information is plotted over one excitation cycle. Studying the figures, both of the contact strips sides are seen to impact with the lower limit and typically lose contact with the excitation after the excitation's lower turning point. For cs_b , additional contact losses occur after the turning point. The contact losses have its origin in a phase difference

between the motions of the contact strips and the head frame, where the head frame is slightly delayed in comparison with the excitation and the strips. The oscillation present in the orbits is a frictional effect and the contact strips has a similar response, an effect even more pronounced in the next example at 6Hz, see figure 6. Now the excitation is in contact during the whole run and a marked decrease in the amplitude of the motion is noticed for cs_{fr} and cs_{bl} . The decrease in amplitude is related to the contact strips rotational natural frequency and will be discussed more in detail later. The inward bend in their orbits, has its origin in the other side's impact with the lower limit.

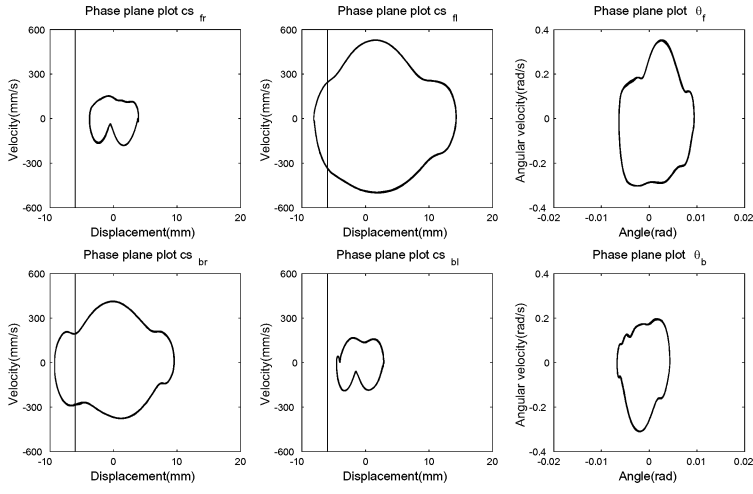


Figure 6. Case 1, 6.0Hz

In the third example at 8.3Hz, repeated contact loss occurs at the excitation before, at and after its lower turning point, see figure 7. The loss is, again, due to a phase difference in the motion between the head frame and the excitation, where the frame still moves downwards whilst the strips and excitation moves upward. The response of the strips has a period that repeats once every second excitation cycle, i.e. they have undergone a period doubling, and behave almost like single degree of freedom systems, due to their small angular motion.

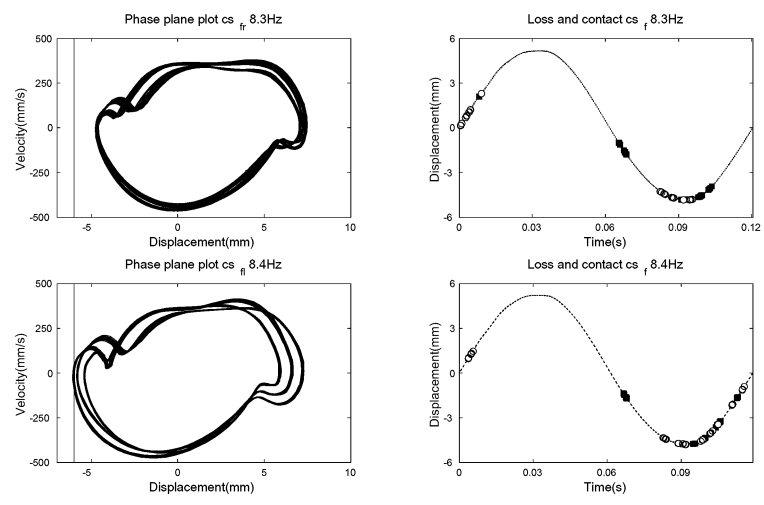


Figure 7. Case 1, 8.3Hz and 8.4Hz

When the frequency is increased to 8.4Hz, the response has become 3 periodic, again as a result of repeated impacts with the excitation, see figure 7.

In figure 8 at 9.2Hz, the attractor looks chaotic and the strips repeatedly impacts at the excitation and the lower stops.

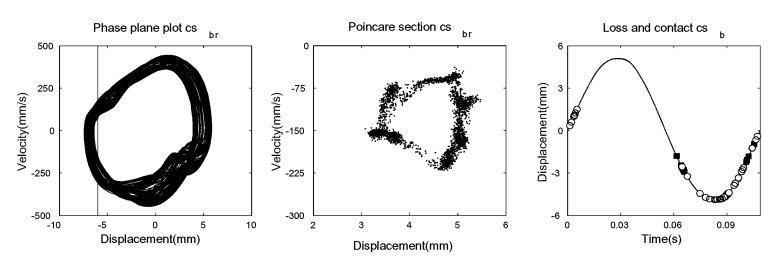


Figure 8. Case 1, 9.2Hz

Figure 9 shows the last results to be presented for the full system and comes from measurements performed before sensors, indicating contact at limits and excitation, were added to the experimental set-up. The results consider the head frame's amplitude response and allow an investigation of the frame assembly's importance over the frequency interval investigated. The change in the set-up, caused by taking the pantograph apart and adding the sensors, affected the pantograph's behaviour at certain frequencies, but the major characteristics of the results presented in figure 9 remains. Analysing the figure, three different peaks occur in the measured data, with the maximum amplitudes in the region 3.5-4Hz. The amplitudes, in this region, vary between $A\approx 9-11$ mm for the different corners of the head frame, with a larger response for hf_{fr} and hf_{fl} than hf_{br} and hf_{bl} . This corresponds to an angular motion of the head frame around its y-axis, as specified in figure 1. The large amplitudes is a result of the

contact strips and springs translational natural frequency, which relates to the undamped natural frequency as: $w_t^2 = k/m$, Tedesco et al. [12]. Using the parameters from the measurements presented in section 4, the resulting frequency $w_n=4.1$ Hz is found in agreement with the results presented here.

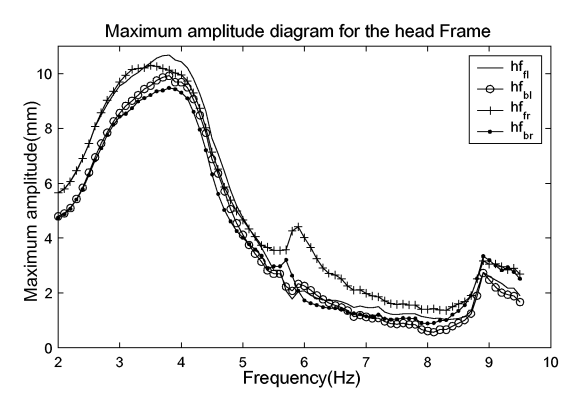


Figure 9. Maximum amplitude diagram for the head frame

The second peak, just below 6Hz, is an effect of the strips rotational natural frequency, which relates to the undamped natural frequency as: $w_r^2 = 2kL^2/I$, Tedesco et al. [12], resulting in $w_n = 5.0$ Hz. At this peak the maximum amplitudes are found for hf_{fr} and hf_{br} , corresponding to an angular motion of the head frame around its x-axis. The third peak at 9Hz could possibly be due to excitation of a natural frequency in the pantograph or caused by impact between the strips and excitation.

5.2 Case 2

In Case 2, the configuration of the contact strips, with different equilibrium points for the strips, resulted in non-impacting motion with the upper limit for cs_f . Since the behaviour of the strip, whilst impacting with the upper limit, is the scope of this case, cs_b is considered in the presented results. The results showed a strong correlation between the strips motions, indicating the possibility that dynamics was transferred between the two via the excitation beam. This is an effect accounted for in Case 3 by removing cs_f .

In the first measurement at 6Hz, figure 10, the response is a periodic motion with repeated contact loss between the strip and excitation, before and after the excitation's upper turning point, and results in an inward bend in the orbit. The vertical line in the phase plane plots indicates the position of the upper limit.

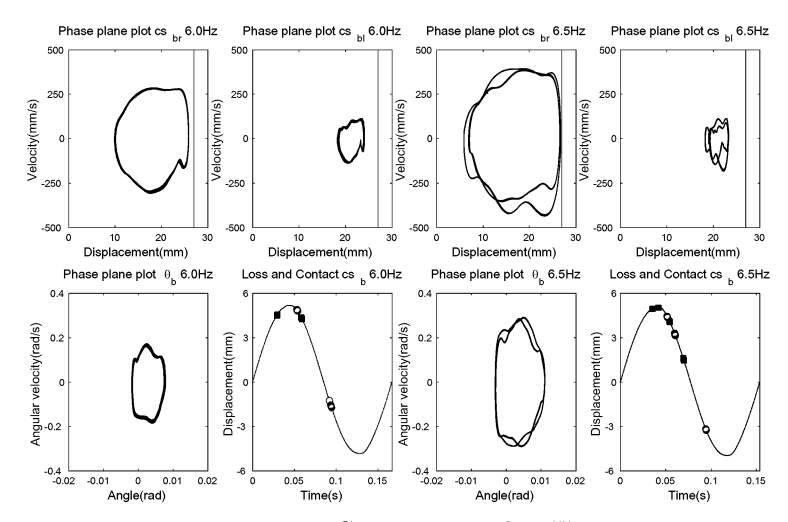


Figure 10. Case 2a, 6.0 and 6.5Hz

The decrease in amplitude, earlier reported for Case 1 in figure 6, is now seen for the contact strip's left side. When the frequency is increased to 6.5Hz, the motion has undergone a period doubling, possibly caused by repeated contact losses at the excitation or the left strip side's impact with the upper limit.

Analysing the results from 7.0Hz in figure 11, contact losses typically occur at and after the excitations upper turning point, and the contact strip repeatedly impacts at the upper limit.

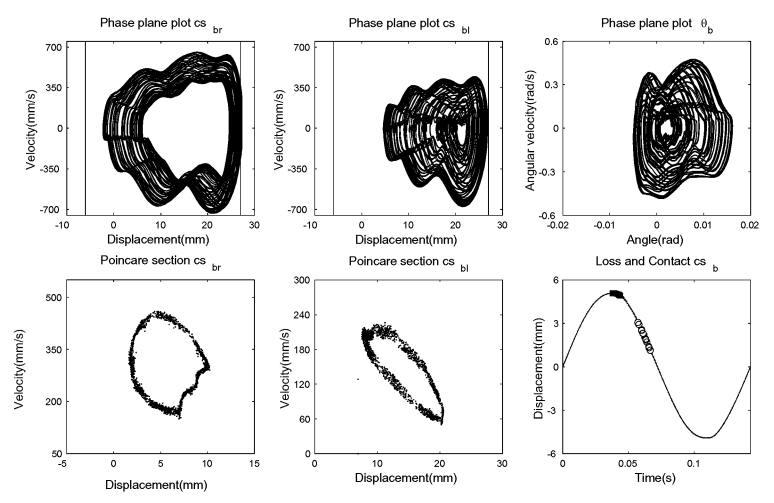


Figure 11. Case 2a, 7.0Hz

The impacts results in a motion that looks quasiperiodic or chaotic, to be studied more in detail in section 6.

If the amplitude is increased to A=10mm, referred to as Case 2b, and the

strips excited at a frequency of 6.8Hz, the resulting motion looks chaotic. Both strip ends impacts with the upper limit and repeated contact loss occur at the excitation, see figure 12.

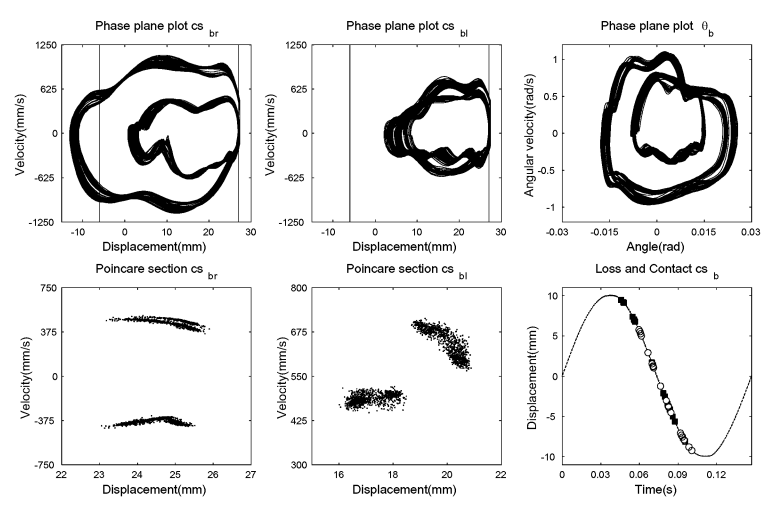


Figure 12. Case 2b, 6.8Hz

5.3 Case 3

The focus of this case is on the behaviour of the contact strip when impacting with the lower limit, and can be seen as a simplification of Case 1, which considered the full rig. Here cs_f has been removed so that no dynamics, possibly transferred between the two contact strips via the excitation beam, affects the measurement. In the first results presented, figure 13, the excitation frequency is 0.4Hz and the friction in the suspensions introduces an oscillation in the velocity data of the phase plane plots. A more indicated jump in velocity is seen for the left side as an effect of the larger friction force present in that suspension, as previously concluded in section 4.

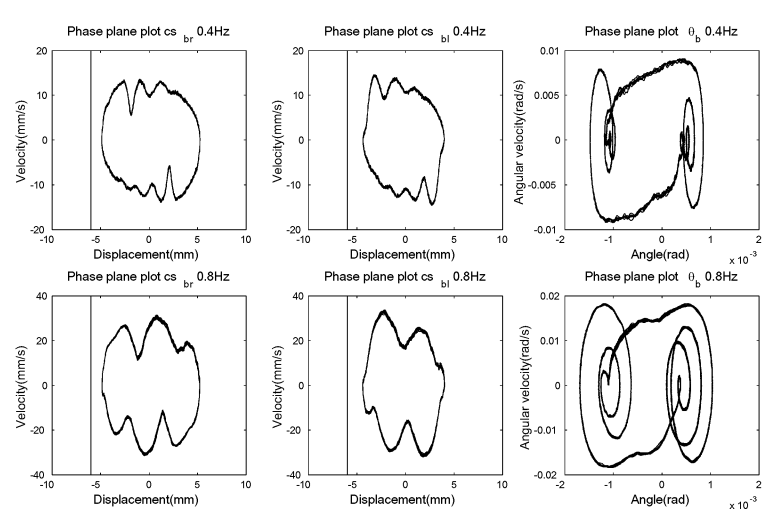


Figure 13. Case 3, 0.4Hz and 0.8Hz

There is up/down symmetry in the contact strips displacement, clearly seen from phase plane plot of the angular motion, and no loss or impact occur at the excitation and lower limit at this frequency. The same applies to the results at 0.8Hz and the results in figure 14, at 1.6Hz and 2.0Hz, with an approximate symmetry remaining.

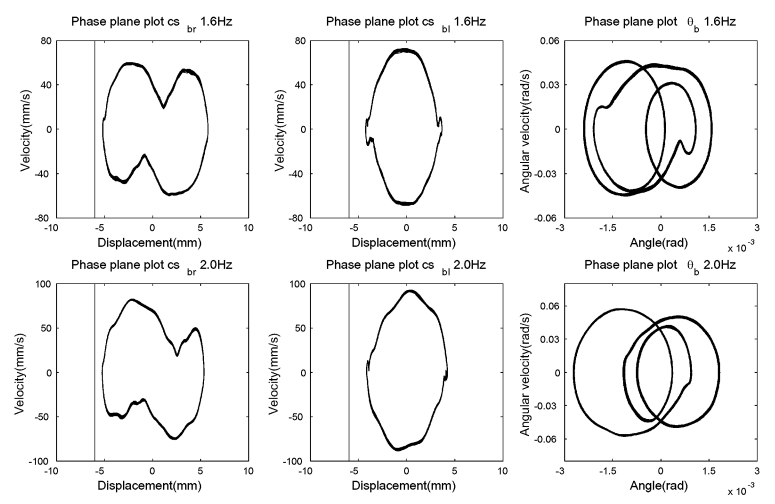


Figure 14. Case 3, 1.6Hz and 2.0Hz

At 3Hz the symmetry breaks down, as seen in figure 15. The angular phase plane plot clearly visualizes this, and the underlying reason is not obvious from the measurements.

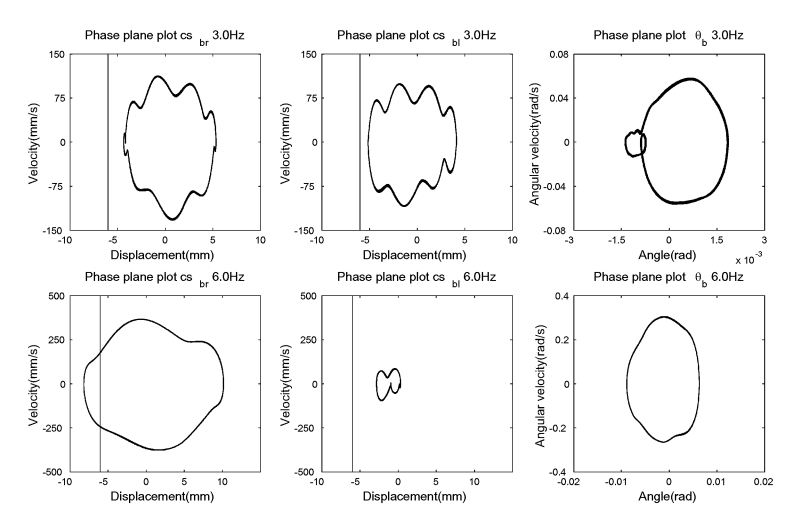


Figure 15. Case 3, 3.0Hz and 6.0Hz

At 6.0Hz the right side impacts with the lower limit, resulting in an inward bend in the left side's orbit. This as well as the marked decrease in amplitude, for the opposite side to the impacting, are recognised from previous cases and are more or less identical to the behaviour found at 6Hz for Case 1, as seen in figure 6.

Analysing the measurements at 9Hz in figure 16, repeated losses with the excitation, before and after the excitations lower turning point, occur and the lower limit is reached at both sides of the strip.

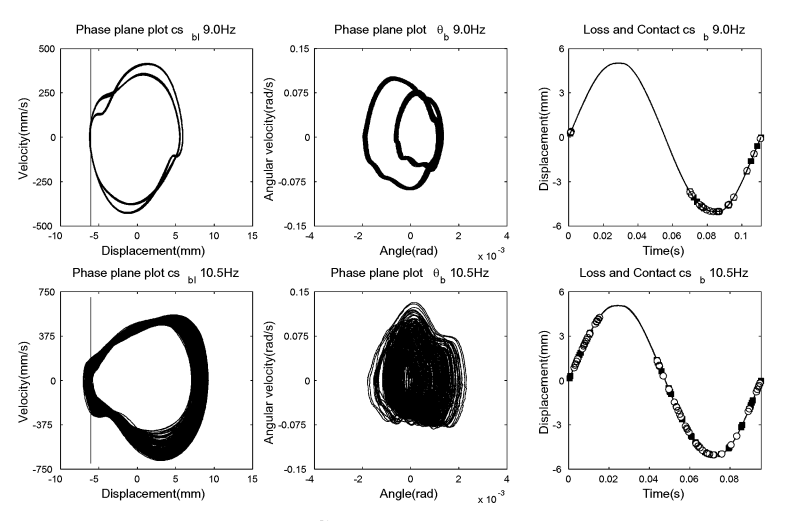


Figure 16. Case 3, $9.0\mathrm{Hz}$ and $10.5\mathrm{Hz}$

It is likely that the impact at the excitation point causes the period doubling

in the motion of the strip, since contact with the lower limit has previously not affected the period. If the frequency is increased to 10.5Hz the motion looks chaotic, with repeated impacts at the excitation and at the lower limit. Studying the signals from the laser measurements in figure 17, the beam centre's motion is seen to differ from the excitation's. The oscillation at 6Hz is recognised from other measurements as well, and is possibly caused by bending of the contact strip or excitation of a natural frequency in the system providing excitation to the pantograph. To be able to conclude the actual reason for this behaviour, there is a need for additional measurements of the excitation beam's ends.

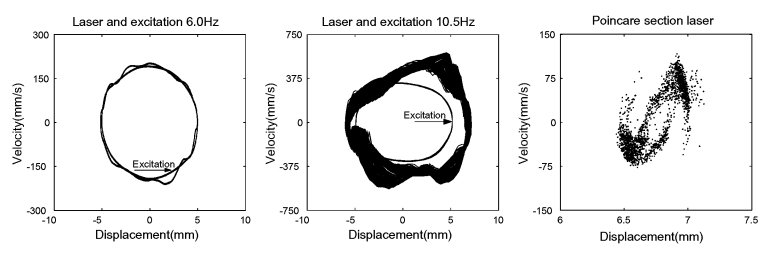


Figure 17. Case 3, 6.0Hz and 10.5Hz

The jumps in the velocity field, at 10.5Hz, has its origin in the impacts with the excitation, and the Poincaré section reveals the fractal structure of the attractor and argues for a chaotic motion of the strip.

6 Modelling and Simulation

6.1 Mathematical Model

The mathematical model represents the head assembly, when fixed to ground, without considering the importance of the frame assembly, and corresponds to the experimental Case 3. The reason to restrict the model to the head assembly, with only one contact strip, is that it is desirable to find out whether a simple model could be used to get a better understanding for the underlying reasons of the pantographs complex behaviour.

The model is built up by a rigid beam, with vertical and rotational freedom around its centre of mass, suspended at its ends in suspension elements, as seen in figure 18. The model is here seen from front, i.e. what appear to be the right side is actually the left side. The suspensions are built up by piecewise linear springs, friction and viscous damping elements.

The piecewise linearity of the springs is introduced into the model by the additional springs placed at each side of the beam's ends. The upper limit is reached when the beam is displaced by x_u in upward direction about its equilibrium position, with the corresponding stiffness k_u , and the lower limit at x_l in downward displacement, with stiffness k_l .

The friction force is modelled by a hyperbolic tangent function, to soften up the step change in friction force, so that the numerics run more efficient and the viscous damping with a hyperbolic cosine function in the denominator. The hyperbolic cosine function causes a decrease in damping force with increased velocity, and is a result of fitting the numerical results to the experimental.

The beams angular displacement is assumed to be small, whereby linearization of the equations has been performed, and the forces acting in the horizontal direction are neglected.

To include the beam centre's oscillation, present in the phase plane orbits from the experimental measurements as seen in figure 17, an additional mass, m_2 , with vertical freedom, is added at the beam centre. Its mass and spring stiffness is matched with a natural frequency in the beam, found at 50Hz.

The excitation of the model is sinusoidal and applied at the beam centre through a stiff mass-less spring and damper element, which applies a force to the mass, m_2 , when in contact with the excitation, and allows loss of contact and impact.

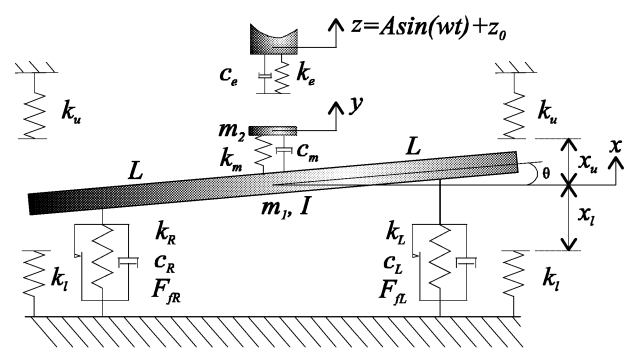


Figure 18. Schematic drawing of the mathematical model, with significant parameters

The mathematical model can be derived using three ordinary differential equations and switching conditions, when loss or impact occurs at the excitation as well as at the upper- and lower limits

$$\ddot{\theta} = L(F_R - F_L)/I \tag{1}$$

$$\ddot{x} = (F_m - F_L - F_R)/m_1 \tag{2}$$

$$\ddot{y} = (-F_m - F_{impact})/m_2 \tag{3}$$

$$z = A\sin(wt) + z_0 \tag{4}$$

where

$$F_L = x_L \cdot k_L + \dot{x}_L \cdot c_L / \cosh(\dot{x}_L \cdot \alpha) + F_{f_L} \cdot \tanh(\dot{x}_L \cdot \beta) + F_{k_{Ll}} + F_{k_{Lu}}$$
 (5)

$$F_R = x_R \cdot k_R + \dot{x}_R \cdot c_R / \cosh(\dot{x}_R \cdot \alpha) + F_{f_R} \cdot \tanh(\dot{x}_R \cdot \beta) + F_{k_{Rl}} + F_{k_{Ru}}$$
 (6)

$$F_m = k_m \cdot x_{yx} + c_m \cdot \dot{x}_{yx} \tag{7}$$

$$F_{impact} = \begin{cases} -k_e \cdot x_{zy} - c_e \cdot \dot{x}_{zy} & \text{when } x_{zy}, \ \dot{x}_{zy} < 0 \\ -k_e \cdot x_{zy} & \text{when } x_{zy} < 0 \text{ and } \dot{x}_{zy} > 0 \\ 0 & \text{when } x_{zy} > 0 \end{cases}$$
(8)

and

$$F_{k_{Ll}} = (x_L + x_l)k_l \text{ when } x_L < x_l \text{ otherwise } F_{k_{Ll}} = 0$$
(9)

$$F_{k_{Rl}} = (x_R + x_l)k_l \text{ when } x_R < x_l \text{ otherwise } F_{k_{Rl}} = 0$$
(10)

$$F_{k_{Lu}} = (x_L - x_u)k_u \text{ when } x_L > x_u \text{ otherwise } F_{k_{Lu}} = 0$$
(11)

$$F_{k_{Ru}} = (x_R - x_u)k_u \text{ when } x_R > x_u \text{ otherwise } F_{k_u} = 0$$
(12)

$$x_R = x - \theta \cdot L \tag{13}$$

$$x_L = x + \theta \cdot L \tag{14}$$

$$x_{yx} = y - x \tag{15}$$

$$x_{zy} = z - y \tag{16}$$

6.2 System Specification

The parameters used in the numerical simulations comes from section 3, and the excitation suspension is modelled using a stiff spring and high damping coefficient, with values as presented in table 2.

Parameter	Value	Parameter	Value
$\overline{m_1}$	3kg	F_{f_R}	1.0N
I	$0.78kgm^2$	k_u	47500N/m
L	0.58m	k_l	7550N/m
k_L	1150N/m	x_u	0.002m
k_R	1150N/m	x_l	0.029m
c_L	16Ns/m	m_2	0.5kg
c_R	10Ns/m	k_m	50000N/m
α	40	c_m	50Ns/m
β	10000	k_e	150000N/m
F_{f_L}	1.6N	c_e	150Ns/m
A	0.005m		

Table 2. The parameters for the numerical model

6.3 Numerical Results

Two different cases, comparable with the experimental, are considered in the numerical analyses of the model built. The first Case A is to be compared with the experimental results from Case 1 and 3, where impact with the lower limit could occur, with $z_0 = 0.022 \mathrm{m}$ causing a preload in each suspensions of $F_p = 25.3 \mathrm{N}$. In the second Case B, one side of the beam is allowed to impact at the upper limit, as in the experimental Case 2, and with $z_0 = 0.005 \mathrm{m}$, resulting in a preload of $F_p = 5.75 \mathrm{N}$. The initial conditions for the two cases are seen in table 3, and the equations solved using the Matlab software package's ode45 solver with a relative and absolute tolerance of $1 \cdot 10^{-9}$.

Case	x(0)	$\dot{x}(0)$	$\theta(0)$	$\dot{\theta}(0)$	y(0)	$\dot{y}(0)$
A	-0.022	$A \cdot w$	0	0	-0.022	$A \cdot w$
В	-0.005	$A \cdot w$	0	0	-0.005	$A \cdot w$

Table 3. The initial conditions for the numerical model

6.3.1 Case A

The first results, presented in figure 19, clearly visualize the frictional effects in the suspensions and the up/down symmetry previously seen in the measurements. The contact at the excitation remains and no impact at the lower limits occur. If compared with the results in figure 13 they show very much the same behaviour.

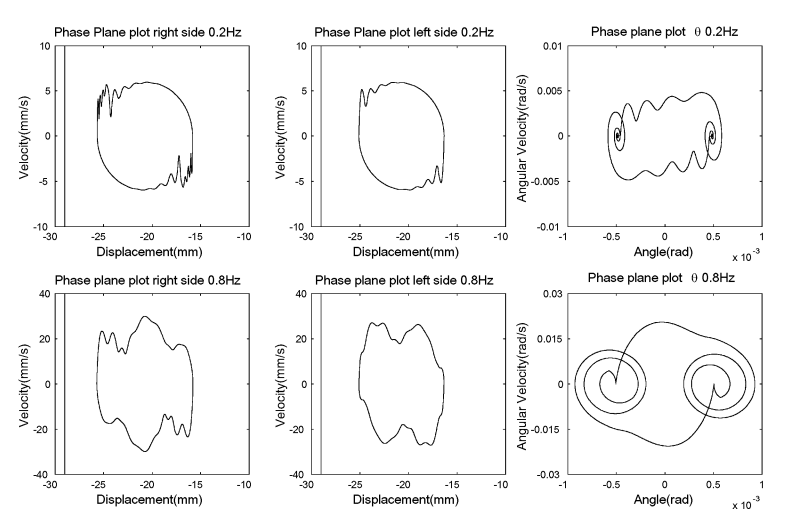


Figure 19. Case A, 0.2Hz and 0.8Hz

The same yields the results in figure 20, to be compared with the experimental results found in figure 14 where the behaviour occurs at a slightly higher frequency.

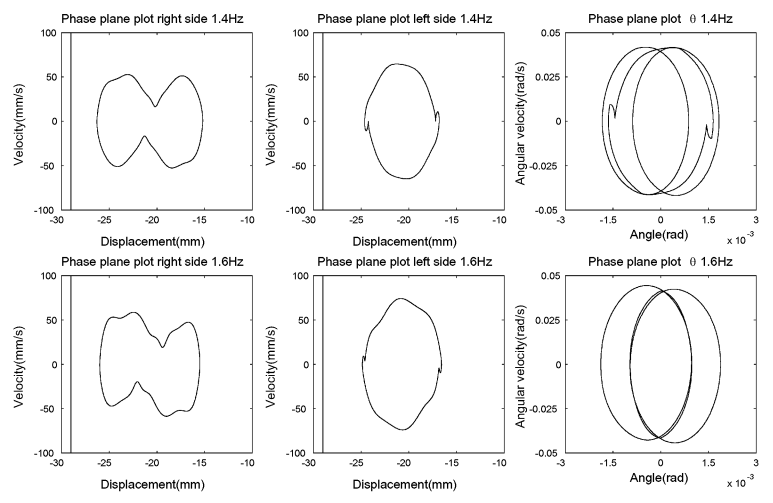


Figure 20. Case A, 1.4Hz and 1.6Hz

At 2.1Hz the symmetry breaks down, but the contact at the excitation remains and no impact with the lower limit occur. The response of the beam's right side is almost the mirrored image of the left, as seen in figure 21, and is similar to the behaviour found at the experimental results in figure 15.

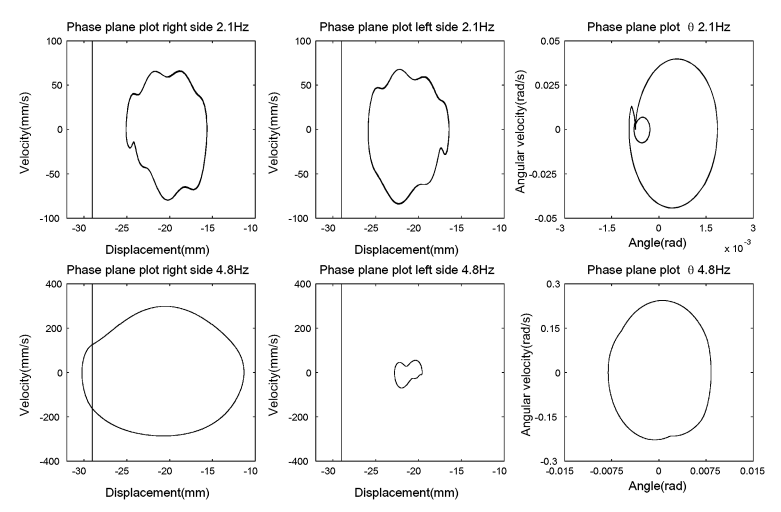


Figure 21. Case A, 2.1Hz and 4.8Hz

The decrease in one side's amplitude, as previously seen in all experimental cases around 6.0Hz, is also found in the numerical simulations, at a frequency of 4.8Hz.

A period doubling occur at 9.4Hz in figure 22, which is at a slightly higher frequency than in the experimental Case 3 in figure 16, caused by the loss in contact and impact at the excitation. When the frequency in increased to 9.6Hz the resulting motion looks chaotic, as an effect of the repeated impacts with the excitation.

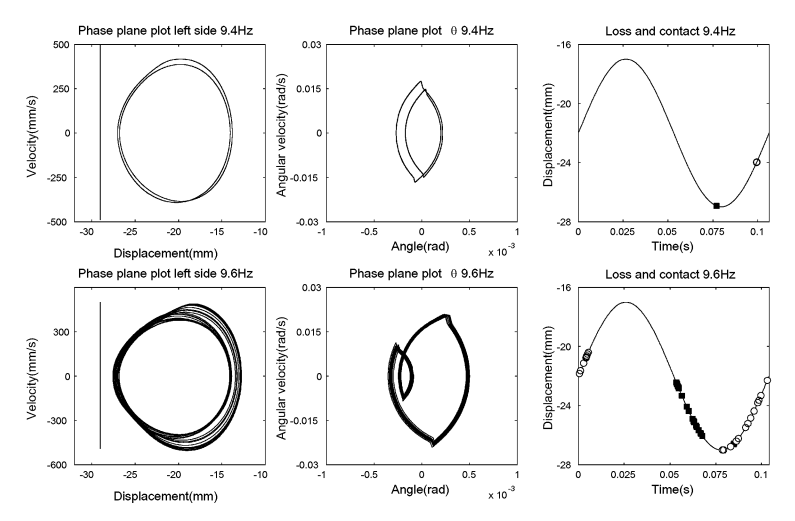


Figure 22. Case A, 9.4Hz and 9.6Hz

Analysing the motion of mass m_2 at 2.1Hz in figure 23 the oscillation in

its orbit, previously seen in the experimental laser measurement in figure 17, is seen. A similar motion occurs at 9.6Hz as for 10.5Hz in the experiment, see figure 17, and the Poincaré section reveals a fractal attractor.

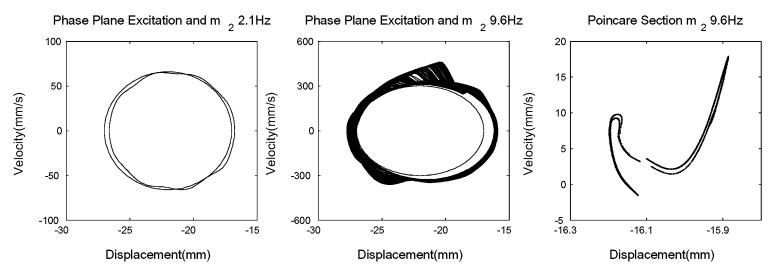


Figure 23. Case A, 2.1Hz and 9.6Hz

6.3.2 Case B

The results in Case B are to be compared with the measurements from Case 2. The response at 4.9Hz in figure 24 is periodic and similar to the experimental results at 6.0Hz in figure 10. If the frequency is increased to 5.1Hz a periodic doubling occur, in agreement with the measurement at 6.5Hz in figure 10.

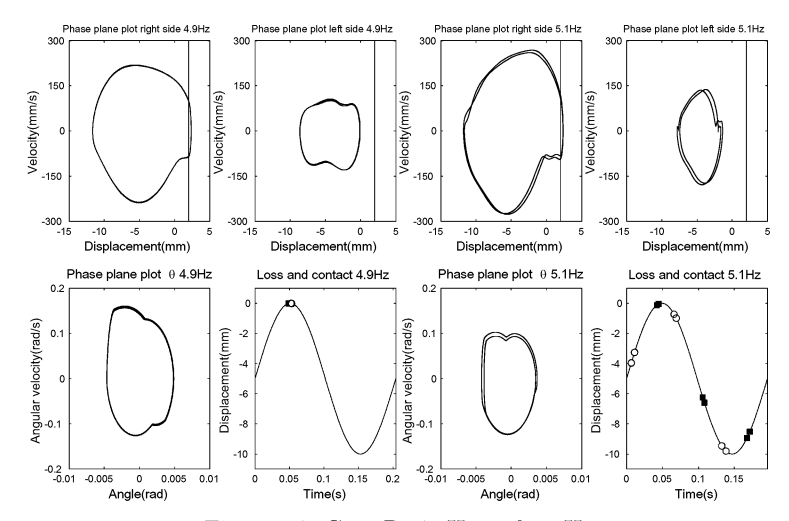


Figure 24. Case B, 4.9Hz and 5.1Hz

The attractors at 5.5Hz, in figure 25, looks chaotic, as found for Case 2b at 6.8Hz in figure 12, and the Poincaré Sections reveals the fractal structure.

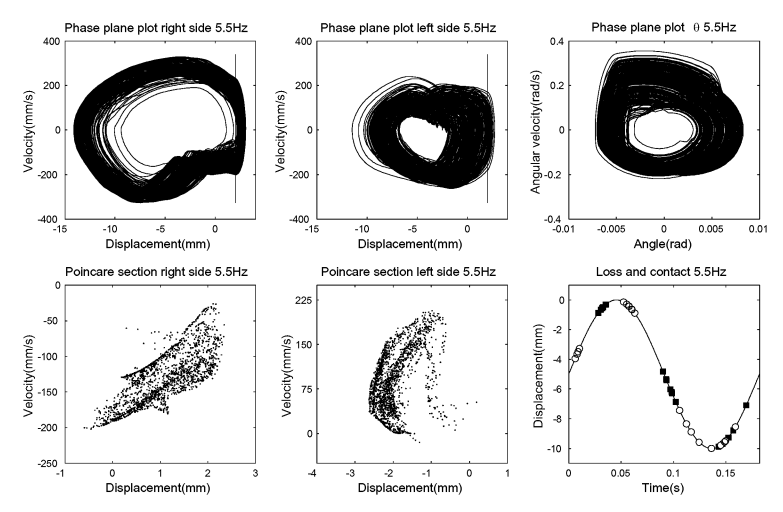


Figure 25. Case B, 5.5Hz

7 Dimension Estimation

When dealing with deterministic dynamical systems it is convenient to classify them according to their dynamical properties, after their transients has died out. The dynamical properties can be described by means of its attractor, which is a set that attracts the motion starting in the region of phase space. From a practical point of view we can divide the attractors into four basic classes: point attractors, limit cycles, N-tori and chaotic attractors. The chaotic attractors can exhibit a very complex and much more irregular structure than the others mentioned, which has led people to call them strange, and are better known as fractals. The first three attractors mentioned can be characterized using traditional linear methods, like a power spectrum, but for the strange attractors nonlinear analysis has to be employed. Frequently used methods for this purpose are dimension and Lyaponov exponents estimation. Fractal dimension estimation is considered here and is a way to quantify the self-similarity of a geometrical object. There are various methods that can be applied for this purpose, see for example Ott et al. [13]. The method used here is the correlation dimension and the approach suggested by Grassberger and Procaccia [14], which has become standard due to its efficiency compared to others. The dimensions of the attractors, as mentioned above, are for the first three an integer value, in comparison with the fractal that has a non-integer value. The achieved value is a measure of the minimum number of states needed to fully uncover the dynamics of the attractor, and for the fractal this value is rounded to the next higher integer.

7.1 Correlation Sum from a Time Series

The Grassberger-Procaccia approach is used to estimate the correlation dimension, as proposed in Kantz and Shreiber [15], and a brief review will now be given. The calculation of the correlation sum involves, by definition, the use of phase space vectors as the location of points on the attractor. In an experimental rig it is seldom the case that all relevant variables can be measured, whereby reconstruction of the full dynamics in an auxiliary phase space is preferable. A single, continuously sampled, time series and the method of delay coordinates is used for this purpose, as introduced by Takens [16]

$$\mathbf{x}_n = (x_{n-(m-1)\tau_d}, x_{n-(m-2)\tau_d}, \dots, x_{n-\tau_d}, x_n), \tag{17}$$

where \mathbf{x}_n is the observable state variable at discrete time n, τ_d is the delay time and m is referred to as the embedding dimension. From these vectors the correlation sum can be formed:

$$C(\varepsilon) = \frac{2}{(N - n_{\min})(N - n_{\min} - 1)} \sum_{i=1}^{N} \sum_{j=i+n_{\min}}^{N} \Theta(\epsilon - ||\mathbf{x}_i - \mathbf{x}_j||), \quad (18)$$

where Θ is the Heaviside step function, $\Theta(x)=0$ if $x \leq 0$ and $\Theta(x)=1$ for x > 0. The estimator counts the pairs $(\mathbf{x}_i - \mathbf{x}_j)$, whose distance is smaller than ϵ , and for a large amount of data $(N \to \infty)$ and small ϵ , the correlation sum is expected to display a scaling

$$C(\varepsilon) \propto \varepsilon^{d_c},$$
 (19)

and the correlation dimension d can be defined as:

$$d_c(N,\varepsilon) = \frac{\partial \ln C(\varepsilon, N)}{\partial \ln \varepsilon},\tag{20}$$

$$d_c = \lim_{\varepsilon \to 0} \lim_{N \to \infty} d(N, \varepsilon). \tag{21}$$

When embedding the reconstructed attractor it is of a major importance to choose a sensible value for the delay time τ_d . There are various suggestions in the literature how to choose this value, but no trivial choice exists. For too small values, problems with strong correlations between successive elements of the delay vectors occur and the vectors x_n will be clustered around the diagonal in the \mathbb{R}^m , unless m is very large. If instead a too large value is chosen, the vectors will be unrelated and the points will fill the \mathbb{R}^m and the fractal structure, which is confined to small length scales, will be destroyed. Here the first zero crossing of the auto-correlation function is used, in combination with visual inspection of the attractor embedded in two-dimensions. Once a value for τ_d is determined, the correlation sum $C(\varepsilon)$ is calculated for increasing values of m. The result is plotted as a log/log plot and a power-law behaviour should be found within some scaling region, typically for a small length scale for experimental data.

The power-law behaviour, which is the signature for self-similarity in the data, can best be found plotting the slope $d_c(\varepsilon)$ of the log/log plot of $C(\varepsilon)$. A plateau in the plot $d_c(\varepsilon)$ then corresponds to the power-law behaviour of $C(\varepsilon)$.

The reason for implementing a delay $n_{\rm min}$, as proposed by Theiler [17], in the start of the second sum in Eq.(18), is that dynamically dependent trajectories otherwise will enter the algorithm. These trajectories have nothing to do with the geometrical structure of the fractal attractor, which is to be evaluated here, and will result in a serious underestimation of the dimension. The value for $n_{\rm min}$ is typically chosen so that a number of cycles are excluded in the estimation.

There is no rule of thumb considering the amount of data, N, to be fed to the algorithm, an issue discussed by Albano et al. [18], since it depends on the structure of the attractor considered and the distribution of the points. Theiler [19] states that "...experience also indicates the need for more experience...", so the only way to be sure that the number of points are enough is to look for convincing evidence of self-similarity in the results.

Noise is another aspect that has to be considered in the estimation, since it will cause the curves to strive towards the embedding dimension for length scales below the amplitude of the noise, and is an issue analysed by Ben-Mizrachi et al. [20] and Argyris et al. [21]. The results indicate that an increase in the estimated dimension occur for noisy attractors. The larger the noise level is in the data the smaller the plateau for $d_c(\varepsilon)$ will be, and if no convincing plateau is found there is a need for noise reduction of the data. Kantz and Schreiber [15] suggests the use of nonlinear noise reduction, to recover the self-similarity of the underlying dynamical system, since linear filtering can artificially increase the measured dimension, Theiler [19].

7.2 Dimension Analysis of Experimental Data

The first data considered is from the measurement at 9.2Hz in Case 1. The data is sampled with approximately 11 points per cycle (ppc) and the total number of data points used is N=60000. The first zero crossing of the autocorrelation function suggests a value for the delay time of $\tau_d=3$, which seems to be a reasonable choice, as seen in figure 26, with a similar look to the original attractor as seen in figure 8. If compared with the attractors reconstructed with a $\tau_d=1$ and 5, that reconstructions are more compressed, whereby $\tau_d=3$ is chosen for the dimension estimate. The algorithm by Kantz and Schreiber [15] allows the user to set the minimum number of reference points, $n_{c \, \text{min}}$, which was chosen to $n_{c \, \text{min}}=58000$. A value $n_{\text{min}}=400$ was used and the embedding dimensions m=2-8 considered. The lines in the correlation sum plot show m=2-8, where the top line is for m=2, the second line m=3 etc. and in the opposite order for the dimension estimate plot.

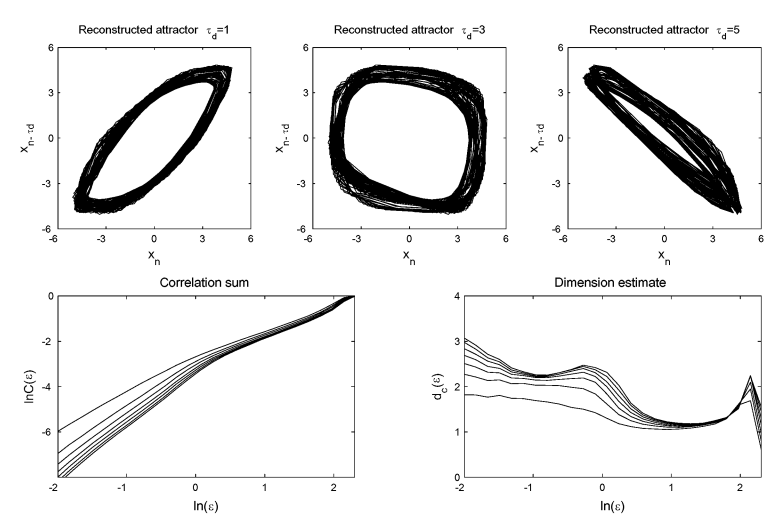


Figure 26. Reconstructed attractors, log/log plot of the correlation sum and the dimension estimate of Case 1 $9.2 \mathrm{Hz}$

Analysing the dimension estimate plot, the size of the attractor introduces a cut-off at the positive end of the $\ln(\varepsilon)$ -axis. In the approximate region $\ln(\varepsilon)\approx 0.5$ to 2 the correlation dimension, d_c , indicates the dimension of the attractors large structure, an orbit with $d_c \approx 1$, before the scaling region, corresponding to the self-similarity of the attractor, is found at $\ln(\varepsilon)\approx 1$ to 0. In this region the curves are found to oscillate around a value of $d_c=2.4\pm 0.1$, and if the curves corresponding to the correlation sum are analysed, they show a power-law behaviour in this region, in agreement with the theory. Below the scaling region the experimental noise causes the curves to strive towards their embedding dimension.

In the next estimation the data from Case 2a at 7Hz is considered, with the approximate sampling of 14ppc and a total of N=60000points. The delay time was chosen to $\tau_d=4$, using the same methodology as above, and the calculation performed with $n_{c\, \rm min}=58000$ reference points and m=2-7. The results are seen in the upper two plots of figure 27, where the scaling region is found between $\ln(\varepsilon)\approx$ -2 and 0. The dimension estimate argues for a correlation dimension just above $d_c\approx$ 2, but a dimension $d_c=2$ is not ruled out. If the dimension is two it would mean that the dynamics is quasiperiodic, and lives on a 2-tori, i.e. the attractor is not a fractal.

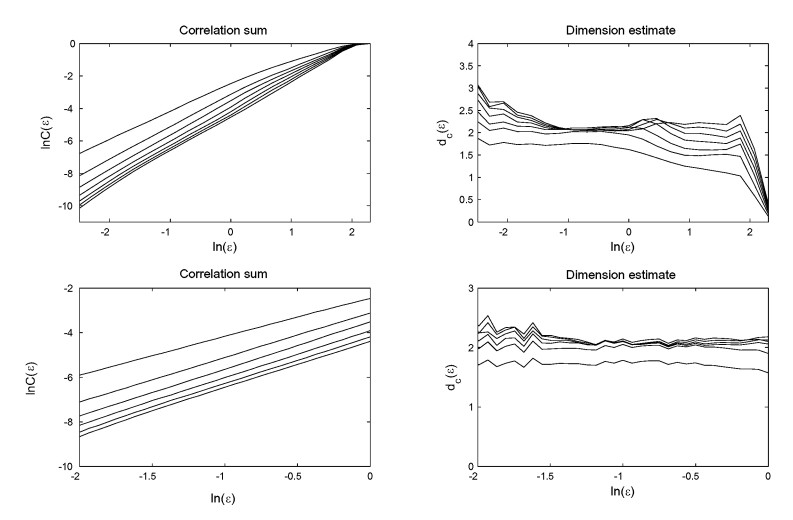


Figure 27. Log/log plot of the correlation sum and the dimension estimate of Case $2a~7.0 \mathrm{Hz}$

To get a better understanding of the dynamics an additional estimation was performed, now with twice the sampling and number of points, with focus on the true scaling region. The delay time is now τ_d =8, the embedding dimensions m=2-7 and the number of reference points is $n_{c\,\mathrm{min}}$ =110000. The results are presented in the second row of figure 27 and argue for a low dimensional chaotic behaviour, with a dimension $d_c \approx 2.1 \pm 0.05$, but the possibility of a quasiperiodic behaviour is not totally ruled out.

In the next estimation the attractor found at 6.8Hz in Case 2b is analysed. The sampling of the data is approximately 42ppc and the number of reference points used $n_{c\,\mathrm{min}} = 80000$. The value for the delay time is $\tau_d = 8$ with $n_{\mathrm{min}} = 2000$ and m = 2-8. Analysing the results in the upper row of figure 28, the dimension estimate again indicates a dimension $d_c \approx 1$ in the large scale region between $\ln(\varepsilon) \approx 0$ and 1. The true scaling region is found below $\ln(\varepsilon) = -1.5$, where the dimension estimation argues for a value just below $d_c = 3$.

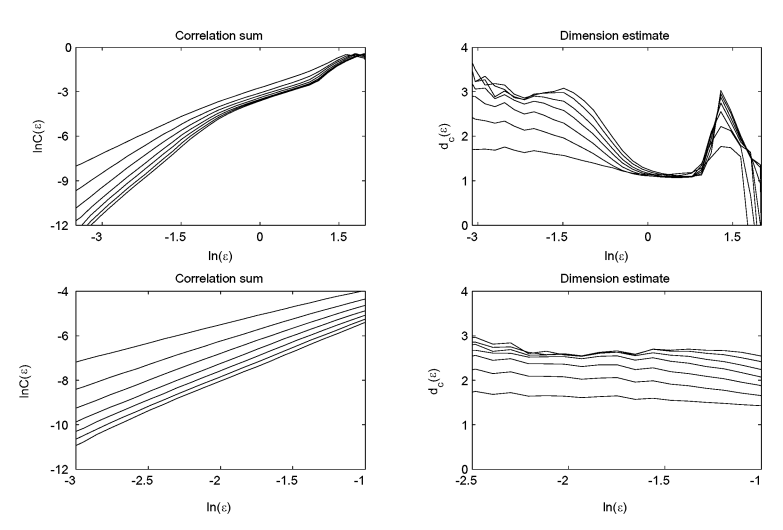


Figure 28. Log/log plot of the correlation sum and the dimension estimate of Case $$2{\rm b}~6.8{\rm Hz}$$

An additional estimation is performed on the same data, now with $n_{c \, \text{min}} = 115000$ points and the scale restricted to the true scaling region. The results are presented in the second row of figure 28 and argues for a dimension $d_c = 2.6 \pm 0.1$.

In the final example of the estimations using experimental data the $10.5 \mathrm{Hz}$ attractor, in figure 17, from Case 3 is considered.

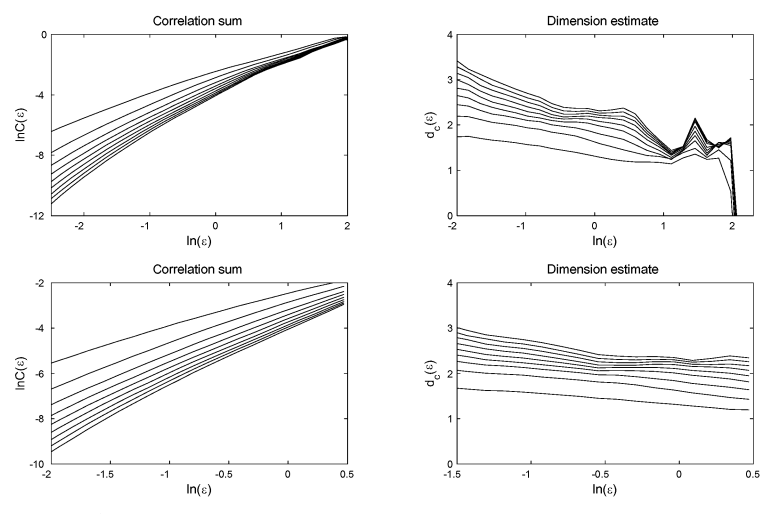


Figure 29. Log/log plot of the correlation sum and the dimension estimate of Case 3 $$10.5{\rm Hz}$$

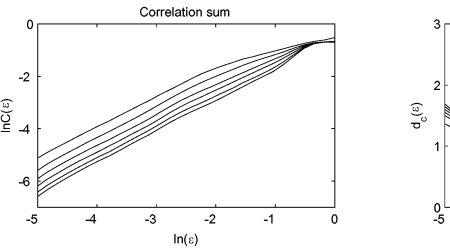
The laser velocity data is used, in comparison with the previous estimations where displacement transducer data was considered. The approximate sampling

of the data is 12ppc, with N=76000 number of points and $n_{c \min}=70000$ reference points used in the analysis. The delay time value was chosen to $\tau_d=3$, and the $n_{\min}=200$ points neglected before starting the second sum of the estimator. The calculation considered the embedding dimensions m=2-10.

The results are presented in the upper two plots of figure 29, and the scaling region found between $\ln(\varepsilon)\approx$ -0.5 and 0.5. Below this region the noise in the data destroys the plateau. The results argues for a dimension d_c =2.3±0.2, which is also true for the estimation in the lower row of the figure. This estimation is performed to see whether a better resolution of the plateau can be found, using twice the sampling, number of points N, reference points $n_{c \, \text{min}}$ and delay time τ_d of the data. The value n_{min} =1000 was used.

7.3 Dimension Analysis of Numerical Data

The dimension estimations performed on the numerical data comes from the attractors at 9.6Hz in Case A and 5.5Hz in Case B. Starting with the 9.6Hz attractor, as seen in figure 23, the Poincaré displacement data is considered. The reason for this is that no reliable estimation results was obtained for the full data set, which might be due to that the trajectories of the attractor rarely visits the regions with fractal structure. When estimating the dimension from a map-like data set, i.e. the sampling is 1ppc, like the one considered, there is no reason to choose a value different to $\tau_d=1$ for the delay time. In the estimation N=11900points are used, neglecting the points from the first five cycles, $n_{\min}=5$, before starting the second sum of the estimator. Embedding dimensions m=2-7 are considered and $n_{c \min}=11800$ reference points searched. The true scaling region is found, see figure 30, between $\ln(\varepsilon)\approx-4$ and -2.5, arguing for a dimension of the Poincaré data $d_c=1.2\pm0.1$, which corresponds to a dimension $d_c=(1+1.2)\pm0.1$ for the underlying dynamical system.



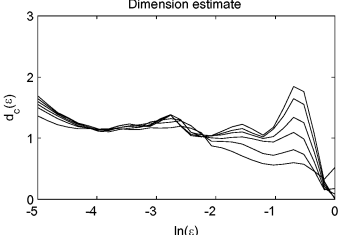


Figure 30. Log/log plot of the correlation sum and the dimension estimate of Case A $9.6 \mathrm{Hz}$

In the second data set, the attractor at 5.5Hz in figure 25 is considered. The data is sampled at 20ppc, with a total of N=100000points, and a delay time $\tau_d=2$ used in the estimation. A value $n_{\rm min}=500$ was chosen and $n_{c\,\rm min}=40000$ reference points searched in the estimation, performed over the m=2-10 embedding dimensions. A convincing plateau is found in the scaling region between $\ln(\varepsilon)\approx$ -1.5 and 0, see the plots in the upper row of figure 31, with a dimension of

approximately $d_c=3.1\pm0.05$. Below the scaling region the plateau, of the curves with embedding dimension m=5-10, is destroyed as a result of too few reference points, but the scaling region is convincing over the interval investigated.

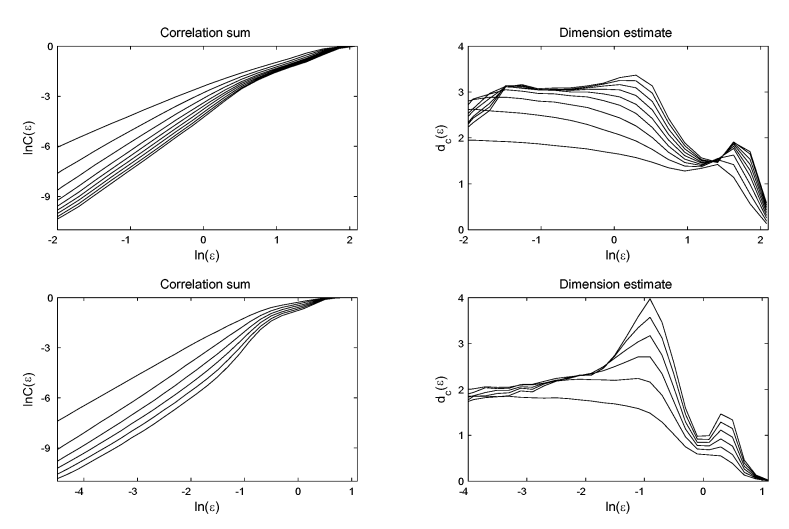


Figure 31. Log/log plot of the correlation sum and the dimension estimate of Case B $5.5 \mathrm{Hz}$

In the lower row of the figure an estimation from the Poincaré data is seen. The number of points used is N=11900, with a delay time $\tau_d=1$, $n_{c\,\mathrm{min}}=11800$, $n_{\mathrm{min}}=5$ and embedding dimensions m=2-7. The signal embedded at m=3 has a scaling region between $\ln(\varepsilon)\approx$ -3 and -1, arguing for a dimension in agreement with the previous estimation. The curves from the embeddings m=4-7 shows a similar result, over a small part of the scaling region, before their plateaus break down.

8 Discussion and Conclusions

The dynamics of a pantograph current collector from a railway train has been studied with the focus on the complex dynamics, better known as chaos, and in particular characterisation of this behaviour using the method of correlation dimension. The system includes several sources for impacts and friction, which are known to cause complex dynamics behaviour in other systems. In the study, experimental measurements were performed of the full pantograph, as well as for a subsystem. The reason for the latter measurements was to provide a better understanding for the behaviour of the pantograph. A mathematical model was developed of the subsystem, based on the experimental investigations, and the results from numerical simulations compared with the experimental. A qualitative good agreement was found between the two, with both systems displaying harmonic, subharmonic, and chaotic responses. The experimental

measurements also indicated quasiperiodic response, but the possibility that it is chaotic is not ruled out.

Frictional effects in the suspension elements were found to be of significant importance at low excitation frequencies e.g. see figure 13 and 19 where also an up- and downward symmetry in the displacement of the contact strip's ends is seen. This symmetry breaks down as the frequency is increased, as seen in figure 15 and 21.

At low excitation frequencies, below 5Hz, the lower frame is highly active with large amplitude responses, due to excitation of a translational natural frequency in the strip/spring configuration. The results from the amplitude responses for the head frame, over the frequency interval investigated, are presented in figure 9.

A peak, related to the excitation of a rotational natural frequency in the strip/spring configuration, is seen just below 6Hz in the figure. The excitation of this natural frequency results in a marked decrease of one side's motion of the contact strip, as seen for the experimental cases in figure 6, 10 and 15, to be compared with the numerical results in figure 21 and 24.

At higher frequencies, the motion of the lower frame will typically be out of phase with the motion of the excitation and the strips, and results in impacts at the excitation at lower frequencies than for the comparable investigation of the subsystem in Case 3. The impacts at the excitation is the major reason for subharmonic and chaotic responses of the contact strip for Cases 1, 3 and A. Examples of the responses are seen in figures 7 and 8, where the contact strips are found to have very small angular displacements and behaves almost like single degree of freedom masses. For Case 2 and B, impacts with the upper limits in combination with impacts at the excitation results in similar responses of the contact strip, as seen in e.g. figures 10 and 11.

An oscillation of the contact strip's centre point was found in the experimental measurements, see figure 17, which is likely to have its origin in bending of the strip. The oscillation is included as an additional mass, at the centre of the strip, in the mathematical model, and the results from simulations showed similar behaviour to the experimental, as seen in figure 23.

The dimension estimations from the experimental chaotic attractors indicate the need for a minimum of three state variables to describe the underlying dynamics of the attractors. This is in agreement with the observation of the chaotic responses of the contact strips in Case 1 and, in particular, for strip in Case 3, which were dominated by translational motion. This argues for the possibility that a second order equation of three state variables could be used to describe the studied motion. In the estimations using numerical data, the dimension of the fractal attractor from Case A was in agreement with the experimental results, in difference with the estimation of the fractal attractor from Case B, which indicated the need for a minimum of four state variables.

The results from experimental and numerical simulations indicate the need to include rotational as well as translational degrees of freedom of the contact strip in a mathematical model of the pantograph. There is also a need to include a representation of the lower frame, and the nonlinearities discussed,

since they highly affect the responses and regions for nonlinear behaviours of the pantograph. The effects possible introduced by bending of the contact strip is not studied in detail, which in combination with the nonlinear characteristics of the lower frame argues for further experimental and numerical investigations of the studied system.

9 Acknowledgements

The financial support from the Swedish National Railway Administration (Banverket) and the Swedish Research Council (VR) is gratefully acknowledged. Schunkgruppen Nordiska AB is also gratefully acknowledged for providing the pantograph used in the experimental investigation.

References

- [1] L. Drugge, T. Larsson, A. Berghuvud and A. Stensson, 'The Nonlinear Behaviour of a Pantograph Current Collector Suspension', DETC99/VIB-8026, Proceedings from ASME Design Engineering Technical Conferences, September 12-15, Las Vegas, Nevada, USA, (1999).
- [2] T. X. Wu and M. J. Brennan, 'Basic analytical study of pantograph-catenary system dynamics', Vehicle System Dynamics, vol.30, pp.443-456, (1998).
- [3] J. Jerrelind and A. Stensson, 'Nonlinear dynamic behaviour of coupled suspension systems', Meccanica, vol.38, pp.43-59, (2003).
- [4] L. Drugge and A. Stensson, 'Modelling and Experimental Evaluation of Catenary Dynamics', Doctoral Thesis, Modelling and Simulation of Pantograph-Catenary Dynamics, L. Drugge, Luleå University of Technology, Luleå, Sweden, ISSN:1402-1544, ISRN:LTU-DT-00/1-SE, (2000).
- [5] S. D. Eppinger, D. N. O'Connor, W. P. Seering and D. N. Wormley, 'Modeling and Experimental Evaluation of Asymmetric Pantograph Dynamics', ASME Journal of Dynamic Systems, Measurement, and Control, vol.110, pp.168-174, (1988).
- [6] W. Seering, K. Armbruster, C. Vesely and D. Wormly, 'Experimental and analytical study of pantograph dynamics', ASME Journal of Dynamic Systems, Measurement, and Control, vol.113, pp.242-247, (1991).
- [7] M. Lesser, L. Karlsson and L. Drugge, 'An Interactive Model of a Pantograph-Catenary System', Vehicle Systems Dynamics, vol.25, pp.397-412, (1996).
- [8] T. Larsson, L. Drugge, 'Dynamic Behaviour of Pantographs due to Different Wear Situations', Computers in Railways VI, Ed. B. Mellitt et al., WIT Press, Southampton, UK, ISBN:1-85312-598-9, pp. 869-880, (1998).

- [9] G. Poetsch, J.Evans, R. Meisinger, W. Kortüm, W. Baldauf, A. Veitl and J. Wallaschek, 'Pantograph/Catenary Dynamics and Control', Vehicle System Dynamics, vol.28, pp.159-195, (1997).
- [10] M. Prącik, K. Furmanik, 'Some problems of modelling and computer simulation of the pantograph and supply contact wire co-operation', 7th Mini Conference on Vehicle System Dynamics, Identification and Anomalies, Budapest, (2000).
- [11] P. Harèll, J. Jerrelind and L. Drugge, 'Experimental measurements of motions in the suspension of a current collector', Licentiate Thesis: Pantograph-Catenary Interaction, P. Harèll, Royal Institute of Technology, Stockholm, Sweden, TRITA-AVE 2004:23, ISSN 1651-7660, (2004).
- [12] J. W. Tedesco, W. G. McDougal, C. A. Ross, 'Structural Dynamics: Theory and Applications', Publisher:Prentice Hall; 1st edition, ISBN: 0673980529, (December 1, 1998).
- [13] E. Ott, T. Sauer, J. Yorke, 'Coping with chaos: analyses of chaotic data and the exploitation of chaotic systems', John Wiley & Sons, Inc. ISBN:0-471-02556-9, (1994).
- [14] P. Grassberger and I. Procaccia, 'Measuring the strangeness of strange attractors', Physica D vol.9, pp.189-208, (1983).
- [15] H. Kantz and T. Schreiber, 'Nonlinear time series analysis', Cambridge Nonlinear Science Series 7. ISBN 0-521-65387-8, (1999).
- [16] F. Takens, 'Detecting strange attractors in turbulence', Lecture Notes in Math. 888, Springer-Verlag, pp.366-381, (1981).
- [17] J. Theiler, 'Spurious dimension from correlation algorithms applied to limited time-series data', Phys. Rev. A, vol.34, pp.2427-2432, (1986).
- [18] A. M. Albano, A. I. Mees, G. C. de Guzman and P. E. Rapp, 'Data requirements for reliable estimation of correlation dimensions', Chaos in biological systems, edited by H. Degn, A.V. Holden and L. F. Olsen (Plenum Press, New York), pp. 207-220, (1987).
- [19] J. Theiler, 'Estimating fractal dimension', J. Optical Soc. Am. A, vol.7, 1055, (1990).
- [20] A. Ben-Mizrachi, I. Procaccia and P. Grassberger, 'Characterization of experimental (noisy) strange attractors', Phys. Rev. A, vol.29, pp.975 - 977, (1984).
- [21] J. Argyris, I. Andreadis, G. Pavlos and M. Athanasiou, 'The influence of noise on the correlation dimension of chaotic attractors', Chaos, Solitions & Fractals, Vol.9, pp.343-361, (1998).

Tryck: Universitetsservice US AB Stockholm 2005 www.us-ab.com